



REPORT

Norwegian GeoTest Sites (NGTS)

ØYSAND RESEARCH SITE: GEOTECHNICAL
CHARACTERISATION OF DELTAIC SANDY-SILTY
SOILS

DOC.NO. 20190154-09-R

REV.NO. 0 / 2019-12-04

Neither the confidentiality nor the integrity of this document can be guaranteed following electronic transmission. The addressee should consider this risk and take full responsibility for use of this document.

This document shall not be used in parts, or for other purposes than the document was prepared for. The document shall not be copied, in parts or in whole, or be given to a third party without the owner's consent. No changes to the document shall be made without consent from NGTS.

Ved elektronisk overføring kan ikke konfidensialiteten eller autentisiteten av dette dokumentet garanteres. Adressaten bør vurdere denne risikoen og ta fullt ansvar for bruk av dette dokumentet.

Dokumentet skal ikke benyttes i utdrag eller til andre formål enn det dokumentet omhandler. Dokumentet må ikke reproduseres eller leveres til tredjemand uten eiers samtykke. Dokumentet må ikke endres uten samtykke fra NGTS.

Project

Project title: Norwegian GeoTest Sites (NGTS)
Document title: Øysand research site: Geotechnical characterisation of deltaic sandy-silty soils
Document no.: 20190154-09-R
Date: 2019-12-04
Revision no. /rev. date: 0

Client

Client: Research Council of Norway (RCN)
Client contact person: Herman Fabrot
Contract reference: RCN project number 245650

for NGTS

Project manager: Jean-Sebastien L'Heureux
Prepared by: santiago Quinteros, Aleksander Gundersen, Jean Sebastien L'Heureux, J. Antonio H. Carraro, Richard Jardine
Reviewed by: Priscilla Paniagua

Summary

This paper describes the geology and geotechnical engineering properties of the fluvial and deltaic gravelly-sandy-silty sediments at Øysand, Norway. Geophysical and geotechnical site investigations carried out between 2016 and 2018 at the site are presented. Field testing included state-of-the-practice and state-of-the-art soil characterisation techniques such as total sounding, seismic cone penetration testing, seismic flat dilatometer, multichannel analysis of surface waves, electrical resistivity tomography, ground penetrating radar, piezometers, thermistors strings, slug tests, and permeability tests using a newly developed CPT permeability probe from NGI. Several sampling techniques were used at the site to assess sample quality. Laboratory testing consisted of index tests and advanced triaxial tests with bender elements to estimate shear strength and stiffness. Data interpretation, engineering soil properties and state variables derived from this analysis are presented, along with comments on data quality. Engineering problems investigated at Øysand so far and discussed in this paper are related to: the impact of using different CPTU types, sample quality assessment by

obtaining soils with state-of-the-practice and state-of-the-art techniques (such as gel push sampler and ground freezing), and frost heave susceptibility.

Contents

1	Introduction	6
2	Regional setting	7
3	Overview of field and laboratory data	8
4	Engineering geology	11
4.1	Deglaciation history and depositional environment	11
4.2	Source of material	11
4.3	Hydrological conditions and stress history	12
4.4	Stratigraphy	13
5	Soil composition	17
5.1	Grain size distribution	17
5.2	Grain angularity	19
5.3	Soil fabric	20
6	Index parameters	21
6.1	Water content	21
6.2	Unit weight of solid particles	21
6.3	Bulk or total unit weight	21
6.4	Indirect estimation of in situ relative density	22
7	In situ testing	24
7.1	Total sounding (TS)	24
7.2	Cone penetration testing (CPTU)	25
7.3	Flat dilatometer (DMT)	27
7.4	Shear wave velocities (v_s) and small strain stiffness (G_{max})	29
7.5	Permeability (k)	31
7.6	Soil temperature	34
8	Advanced laboratory testing	35
8.1	Drained triaxial compression tests	35
9	Engineering parameters	36
9.1	Overconsolidation ratio (OCR)	36
9.2	Coefficient of earth pressure at rest, K_0 , and estimated in situ effective stresses	37
9.3	Effective stress-strength parameters—field and laboratory testing	38
10	Further geotechnical characterisation considerations	41
10.1	Impact of cone penetrometer type on CPTU results	41
10.2	Sample quality research in progress	42
10.3	Frost heave susceptibility of Unit II sandy/silty soils	42
11	Summary and conclusions	43
	Acknowledgments	44
	Conflict of Interest	44
	References	45

Review and reference page

1 Introduction

The research presented in this paper integrates with the Norwegian Geo-Tests Sites (NGTS) project [1], the purpose of which is the development and characterisation of five geotechnical test sites in Norway: a silty sand site at Øysand (this article), a silt site at Halden [2], a soft clay site at Onsøy [3], a quick clay site at Tiller/Flotten [4] close to Trondheim (see Figure 1) and a permafrost site in Longyearbyen, Svalbard [5]. This paper presents the characterisation of the Øysand site.

Silty sand deposits are common in many parts of the world, including rivers, offshore banks and deltaic areas, where many major cities are constructed. Intrinsic properties and state variables affect soil behaviour [6]. Intrinsic properties include mineralogy, particle angularity and surface roughness, gradation (including grain size distribution and its derivatives such as fines content), etc. State variables include relative density (D_r), mean effective stresses (p'), fabric, overconsolidation ratio (OCR) and the coefficient of earth pressure at rest (K_0), and may relate to cementation and ageing. State-of-the-art techniques for characterization and sampling have been applied to estimate the *in situ* soil properties at Øysand. The derived intrinsic and engineering parameters obtained from the field and laboratory testing are summarized in this paper. A link is presented between the geological history and its impact on the engineering parameters, as established through *in situ* and laboratory testing. The geotechnical knowledge acquired at the Øysand research site will contribute to expanding the current understanding of the engineering behaviour of natural silty sandy deposits.

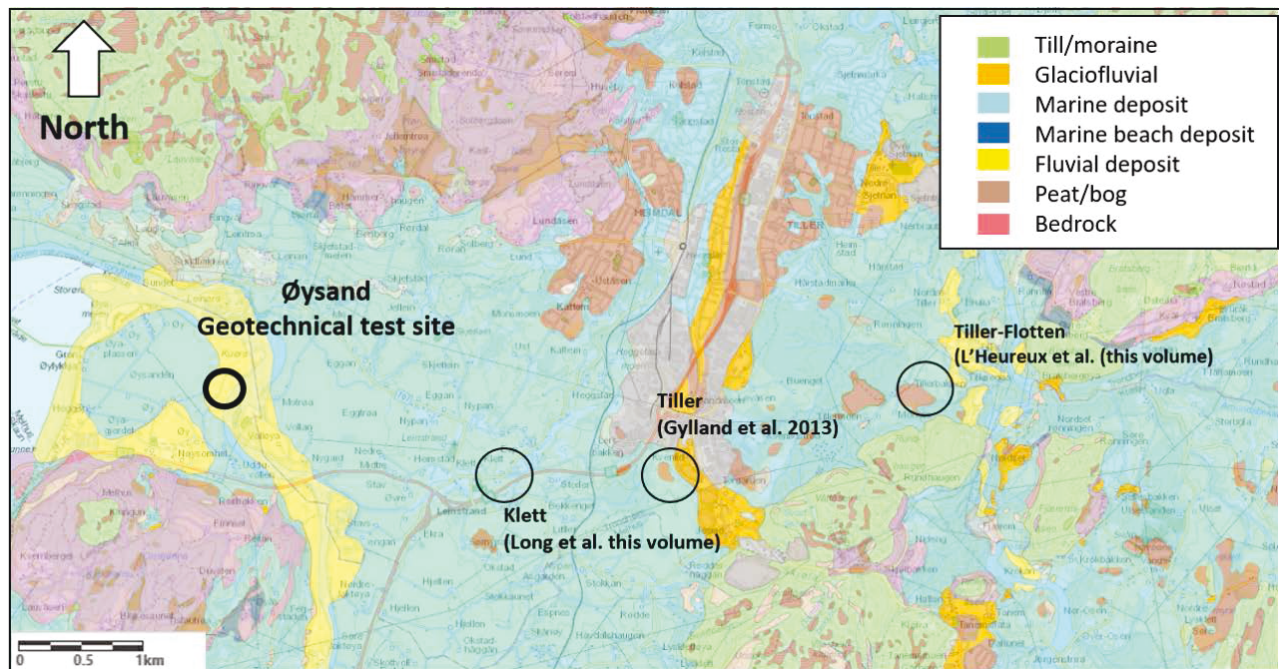


Figure 1. Geological map of Øysand peninsula (data from www.ngu.no).

2 Regional setting

The Øysand site is located about 15 km south-west from Trondheim, Norway (see Figure 2). The sand deposit at Øysand originates from the Gaula River, a 150 km long river with an average discharge of $97 \text{ m}^3/\text{s}$ which flows into the Trondheimsfjord and borders the site to the east, see Figure 2. An area of approximately $35,000 \text{ m}^2$, that is used mainly for agricultural purposes, is available for geotechnical investigations at Øysand. The deposit at the site consist of fluvial material, underlain by deltaic and marine sediments (Figure 2). While the depth to bedrock is unknown, a 1940s investigation made during the German occupation of Norway showed that the sediments extend to a depth of at least 80 m below ground level.

The site topography comprises a practically flat surface that reposes around 2.7 m above sea level, with the exception of a 7 m high ridge along the south part of the field. A road enables access throughout the year. Two farms are located about 500 m south-west of the site.

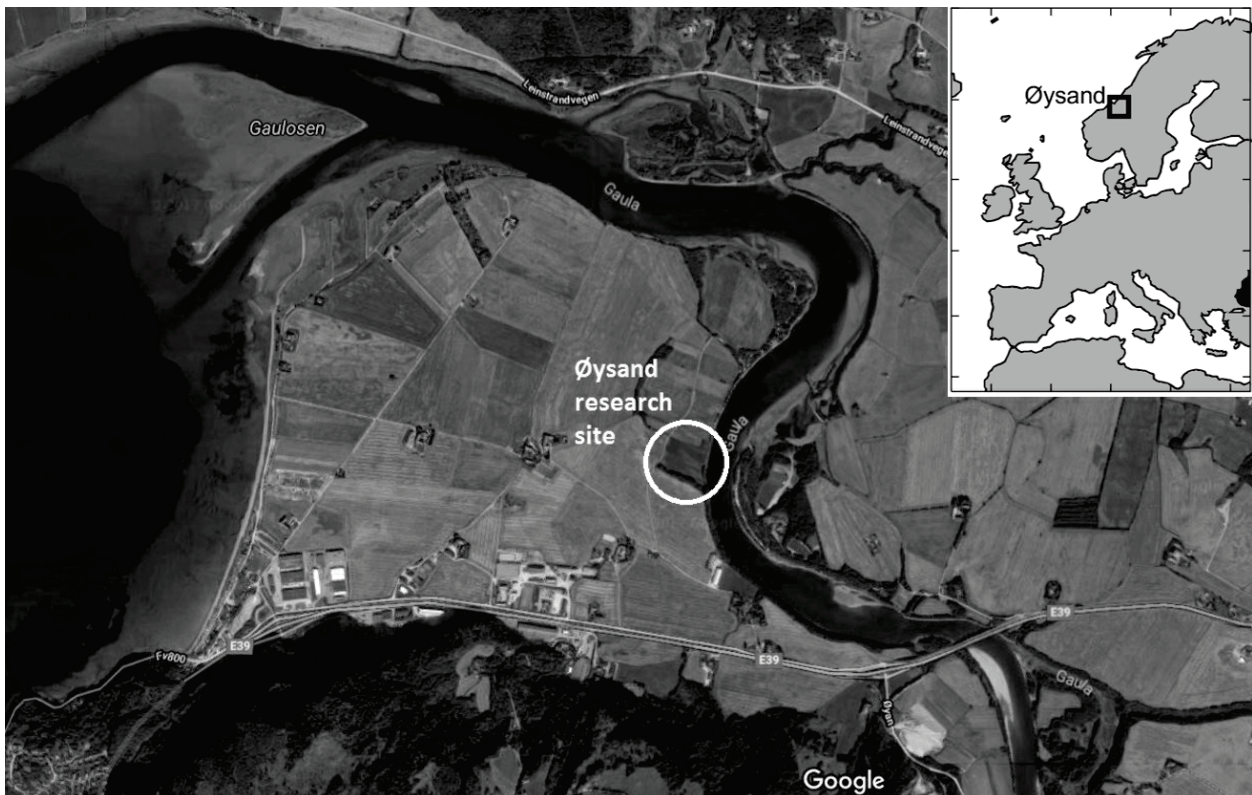


Figure 2. Location of the Øysand research site (modified from Google Maps 2017).

3 Overview of field and laboratory data

Site characterization at the Øysand research facility started in 2016 as part of the Norwegian GeoTest site project (NGTS). A wide range of *in situ* tools, geophysical techniques, sampling techniques and laboratory tests have been used to assess the geological history and geotechnical properties of the sand deposits since 2016. A complete list of all geotechnical work, geophysical investigations, and laboratory tests performed at the site (including tests procedures, references and derived geotechnical parameters) is given in Table 1. The field test locations are shown in Figure 3.

Site characterization at Øysand has involved geophysical and geotechnical techniques. Geophysical tests included: Multichannel Analysis of Surface Waves (MASW), Symmetrical Resistivity Profiling (SRP), Multi-Sensor Core Logging (MSCL), Electrical Resistivity Tomography (ERT), Ground Penetration Radar (GPR) and Self Polarization (SP). Geotechnical tests included: Total Soundings (TS), Cone Penetration Tests (CPTU), Seismic Cone Penetration Test (SCPTU), Seismic Dilatometer Tests (SDMT), Piezometers (Piezo), Thermistors Strings (THS), Slug test (SLU), and Permeability tests using a NGI newly developed permeability probe [7]. Soil was

sampled using the Sonic Drill Sampler (SDS), the Geonor Push Piston Sampler (GPP), an open Push Piston Sampler (PPS), and the Japanese Gel Push Sampler (GPS). Sampling with an *in situ* ground freezing technique was conducted in April and May of 2019.

MSCL results are used for indirect estimation of the water content (w) and unit weight (γ) of the soil. ERT and GPR results were used for interpretation of a 3D geological map of the site and for preliminary assessment of soil layering. ERT and GPR results were also used during the sampling campaigns for identifying the thickest layers of sand for specifying the sampling locations. CPT and DMT results are used for soil classification and for indirect estimation of *in situ* γ , D_r and K_0 . Ground temperature was measured using THS. Permeability was obtained from Slug tests and the NGI permeability probe, respectively, and the results were compared with laboratory tests. Field and laboratory measurements of shear wave velocity from MASW/SCPTU/SDMT and Bender elements (BE) are used for estimating the small strain shear modulus (G_{max}).

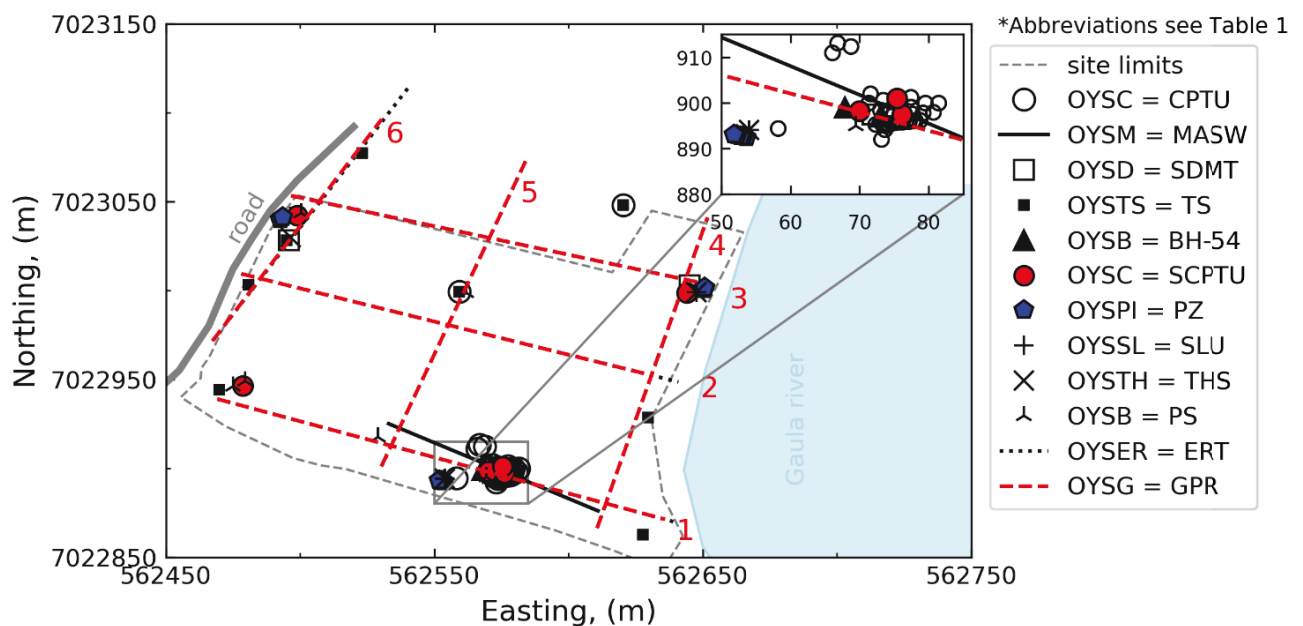


Figure 3. Location of field tests at Øysand research site.

Table 1. Summary of geophysical, in situ and laboratory tests performed at Øysand.

Test	Abbreviation	Measured/Controlled	Interpreted	Reference/Comment
Geophysical/non-intrusive				
Electrical resistivity tomography (ERT)	OYSER	Resistivity	$Z_{bedrock}$, soil type	by NGI ¹
Ground penetration radar (GPR)	OYSG	F_{DT}	$Z_{bedrock}$	by NGI
Multi-channel analysis of surface waves (MASW)	OYSM	v_p, ω	v_s, G_{max}	by APEX ² , and Reykjavik University
In situ				
Total sounding (TS)	OYSTS			
Cone penetration test (CPTU, SCPT)	OYSC	$q_c, f_s, u_2, v_{s,vh}$	$\sigma'_{pr}, G_{vh,max}, \phi'$	
Seismic flat dilatometer (SDMT)	OYSD	$P_0, P_1, I_D, K_D, E_D, v_{vh}$	K_0, σ'_{pr}, ϕ'	
Piezometers (PZ)	OYSPI	u, t	u_0	Pore pressure
Thermistor string (THS)	OYSTH	T, t	-	
Slug tests (SLU)	OYSSL	Pressure head	k	
NGI permeability probe (NGI-flow cone)	OYSC	Flow	k	
Sampling				
Geonor fixed piston composite (PS \varnothing 54 mm)	OYSB_PS54	-	-	2 BH, 12 tubes
Thin wall push piston sampler (PS, \varnothing 72 mm)	OYSB_PS72	-	-	4 tubes
Gel Push Sampler (GPS, \varnothing 72 mm)	OYSB_GPS	-	-	2 tubes
Ground freezing (\varnothing 100 mm)	OYSB_GF	-	-	April & May 2019
Laboratory				
Water content	-	w	-	
Unit weight (density)	-	$\gamma_d, \gamma_t (\rho_d, \rho_t)$	-	
Unit weight of solid particles	-	γ_s	-	
Grain size distribution	-	-	% gravel, sand, silt, clay	
Multi sensor core logging (MSCL)	-	ρ, MS	N	NGU in-house ³
Split core imaging	-	-	-	NGU in-house
Hydraulic conductivity	-	k_v	k_v	
Triaxial test: CAUC, CADC	-	$\varepsilon_a, \varepsilon_r, \varepsilon_p, u, p, q$	$\phi'_{1s}, \phi'_{pr}, E$	
Bender element test (BE)	-	$v_{s,vh}$	$G_{vh,max}$	
Micro computed tomography (CT)	-	-	-	On each tube and specimen

- ¹ NGI = Norwegian Geotechnical Institute, Oslo Norway
- ² APEX = Apex Geoservices, Wexford, Ireland
- ³ NGU= Geological Survey of Norway, Trondheim, Norway (in Norwegian: Norges Geologiske Undersøkelse)

4 Engineering geology

4.1 Deglaciation history and depositional environment

Following deglaciation of the region approximately 10,300 years ago, the study area was subject to glacio-isostatic rebound and fall of relative sea-level. The highest relative sea level of the Øysand area is approximately 175 m.a.s.l. above the current sea level [8]. Throughout the Holocene the mouth of the Gaula River continuously moved in a north-westwards direction in phase with delta progradation. The coarser deltaic and fluvial sediments deposited directly on the seafloor which consisted mostly of silts and clays (marine deposits). A quaternary geology map of the study presented in Figure 1 shows that the entire research site is located on a fluvial deposit reposing on thick deposits of marine clays.

According to the shoreline regression curve for the region [9], the study area probably emerged from the sea only about 1000–1500 years ago. As a consequence, the deltaic sediments at Øysand are fairly young. Following their emergence from the sea, the deltaic deposits were covered by coarser river deposits as the Gaula River meandered in the valley. Coarse sands and gravels are therefore expected to occur in the upper portion of the soil stratigraphy at Øysand.

4.2 Source of material

The catchment area of the Gaula river is 3668 km² and is dominated by rocks from the Caledonian mountain range, including greenstone, amphibolite, tuff, and micaceous shales [10]. The deposits found at Øysand today were produced by glacial erosion of the bedrock and fluvial erosion of marine and glacial deposits in the catchment. The major mineralogical components of the bedrock and glacial deposits in the catchment area are quartz, feldspars, illite and chlorite with the latter making up the main proportion of the clay fraction.

4.3 Hydrological conditions and stress history

A total of 12 electrical piezometers (Geotech PVT with built-in data loggers) were installed in clusters around the site. Their depths range from 5 to 20 m below ground level. One cluster was installed near the Gaula River (OYSPI06–OYSPI10), second cluster (OYSPI01–OYSPI05) is located 160 m to 170 m away from the river in the southern part of the study area, and a third one (OYSPI11–OYSPI12) close to the access road (see Figure 3). The piezometers reveal that the ground water level (GWL) is generally set around 2 m below ground level. Pore pressure measurements taken from May to December of 2017 are shown in Figure 4a with time. Figure 4b shows that the groundwater pressure increases hydrostatically with depth. However, locations near to the river are also affected by neap and spring tides from the nearby Trondheimsfjord, which occur every month and generate cyclic variations of about ± 10 kPa in the pore pressures and hence vertical and horizontal effective stresses.

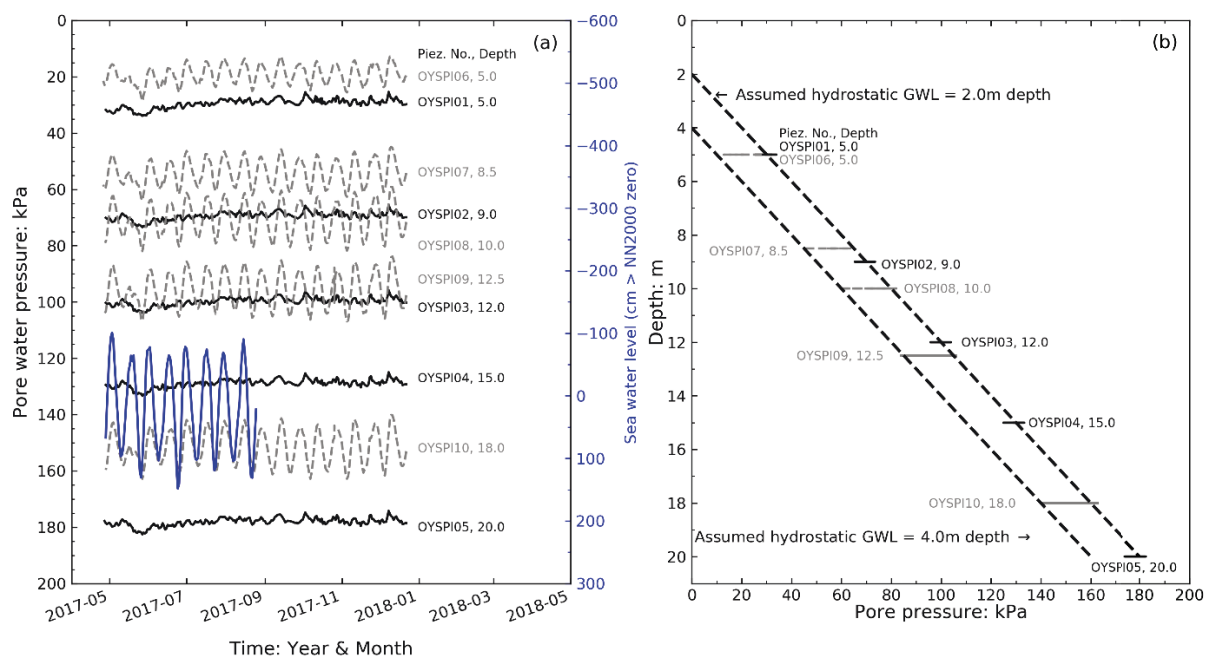


Figure 4. Piezometer results: (a) pore pressure with time, (b) pore pressure with depth.

The 7 m high ridge located in the south of the study area was most likely formed by erosion as the Gaula River meandering across the area (Figure 5). Any such erosion of overlying sediments would have left the sands encountered today in an overconsolidated condition. No other previous loading processes have been identified to date.

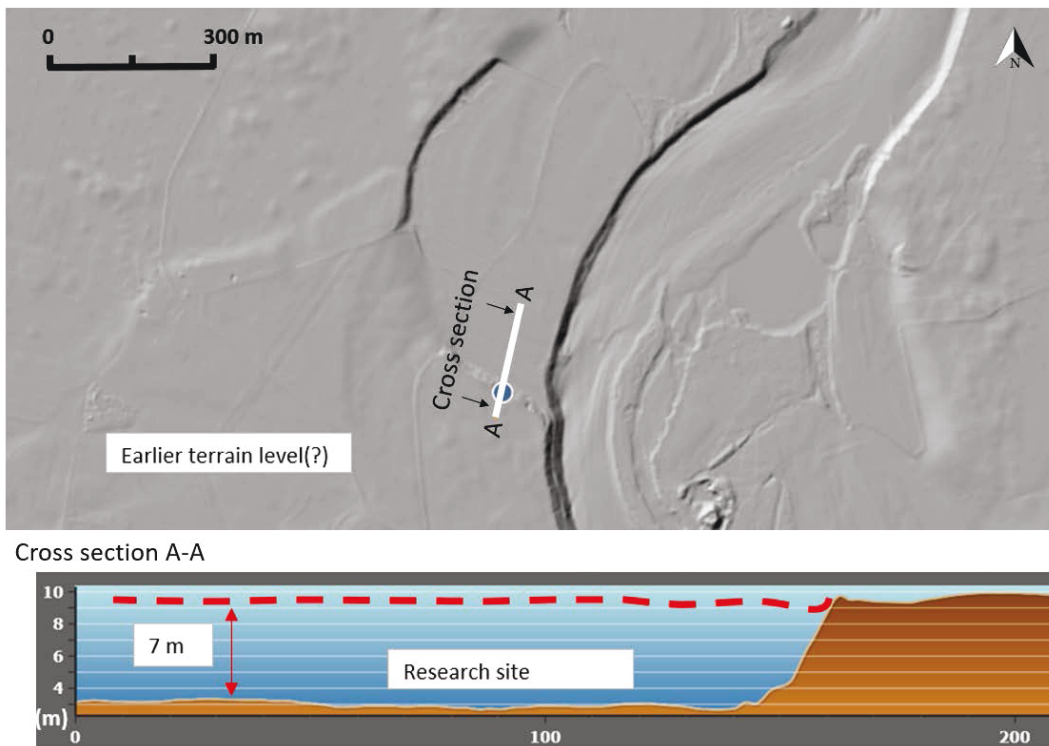








Figure 5. Possible erosion of the site by the Gaula River (data from www.hoydedata.no).

4.4 Stratigraphy

The stratigraphy at the site has been interpreted on the basis of *in situ* soundings, boreholes logs and geophysical data. Due to its geological history, the soil deposit at Øysand presents several layers and significant lateral variability. In general, the stratigraphy down to 20 m below ground surface can be divided into two main units: i) a top 6–10 m of coarse to gravelly sand (fluvial deposit), and ii) a lower unit consisting mostly of fine silty sand (deltaic soils), see also [11]. The lower unit also presents layers of clay and silt. Photographs of typical soil samples at the site, and a description of the soil, are presented in Table 2. Figure 6 shows the material from OYSB09 in the south of the Øysand site. Figure 7 shows a complete borehole log down to 20 m below ground level.

A combined geophysical survey consisting of ERT and GPR was carried out in April 2017. A total of 6 profiles were recorded, exact locations are illustrated in Figure 3. ERT is useful for obtaining 2D and/or 3D maps of the spatial and temporal variation of the soil electrical conductivity, which also correspond to variations in soil water content [12], grain size and pore water chemistry.

Table 2. Summary of Øysand stratigraphy, with photos of selected samples.

Depth range [m]	Soil description [-]	Image [-]
0.0–2.0	SAND, silty, fine, loose to medium dense, with organic material	
2.0–10.0	SAND, fine to coarse gravelly, medium dense, with layers of fine to medium silty sand and traces of organic material	 
10.0–20.0	Depending on the location: Either, SAND, fine to medium silty with thick layers of SILT, sandy, clayey material, medium dense to dense. Or, SAND, fine to medium silty with thin traces of silty material, medium dense	  

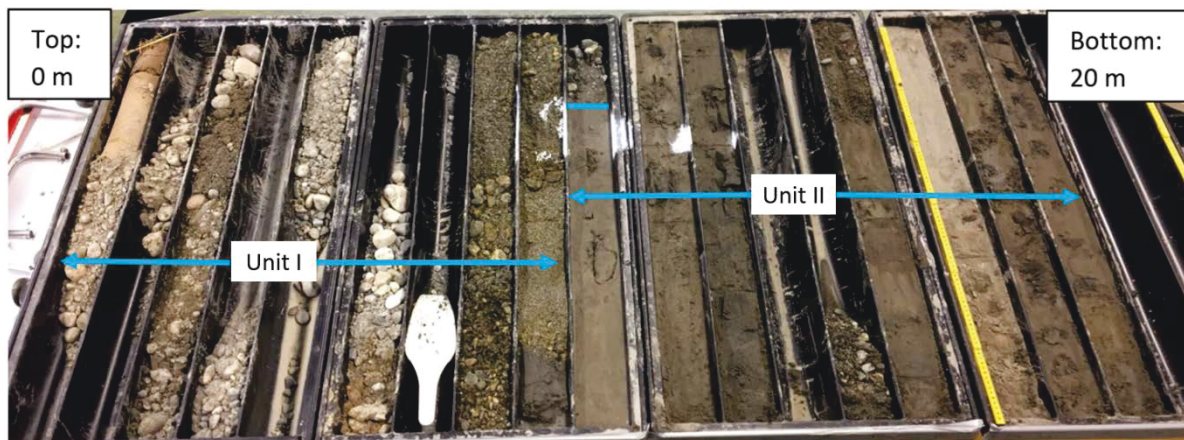
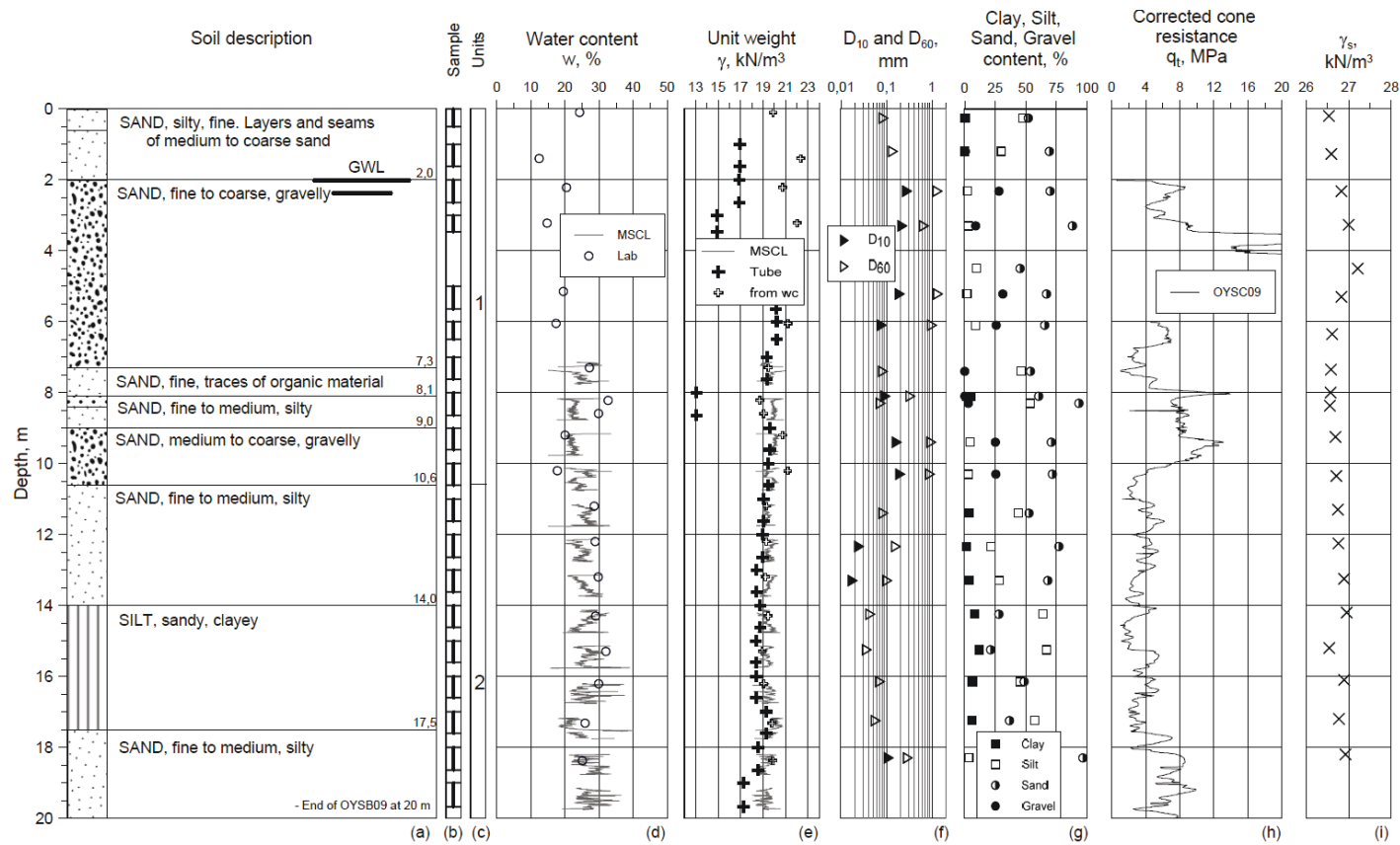


Figure 6. Stratigraphy based on soil sampled towards the south of site (OYSB09).



* Multi sensor Core Logging

** $q_t = q_c + u(1-a)$ after [13]

Figure 7. Borehole log (OYSB09).

ERT results are presented in Figure 8. They show a generally consistent higher resistivity layer down to 10 m below the terrain, which corresponds to the upper coarse to gravelly sand (Unit I). Below this, resistivity decreases gradually from around 250 Ωm down to 50 Ωm in the lower Unit II of silty fine sand. The gradual change in resistivity may be linked to the coarsening upward found in this unit.

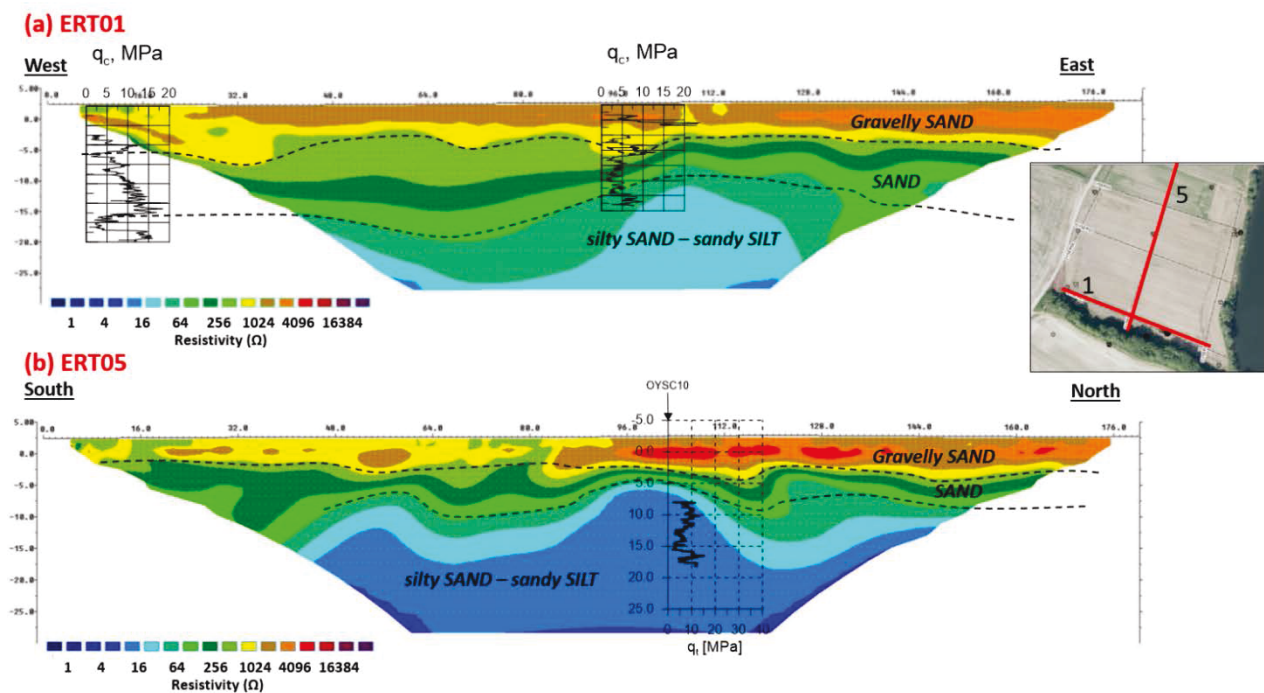


Figure 8. ERT interpretation: (a) ERT01 and (b) ERT05.

Due to the rapid attenuation of electromagnetic waves in the deposit, GPR data provides shallower information than the ERT (down to approximately 6–7 m). Results shown in Figure 9 indicate multiple reflections around 2 m below ground surface. This may correspond to the top of the gravelly soil, but might also be influenced by the groundwater level. Below this the GPR data reflects several layers dipping in a north-westward direction, following the likely direction of delta progradation and the deltaic fore sets.

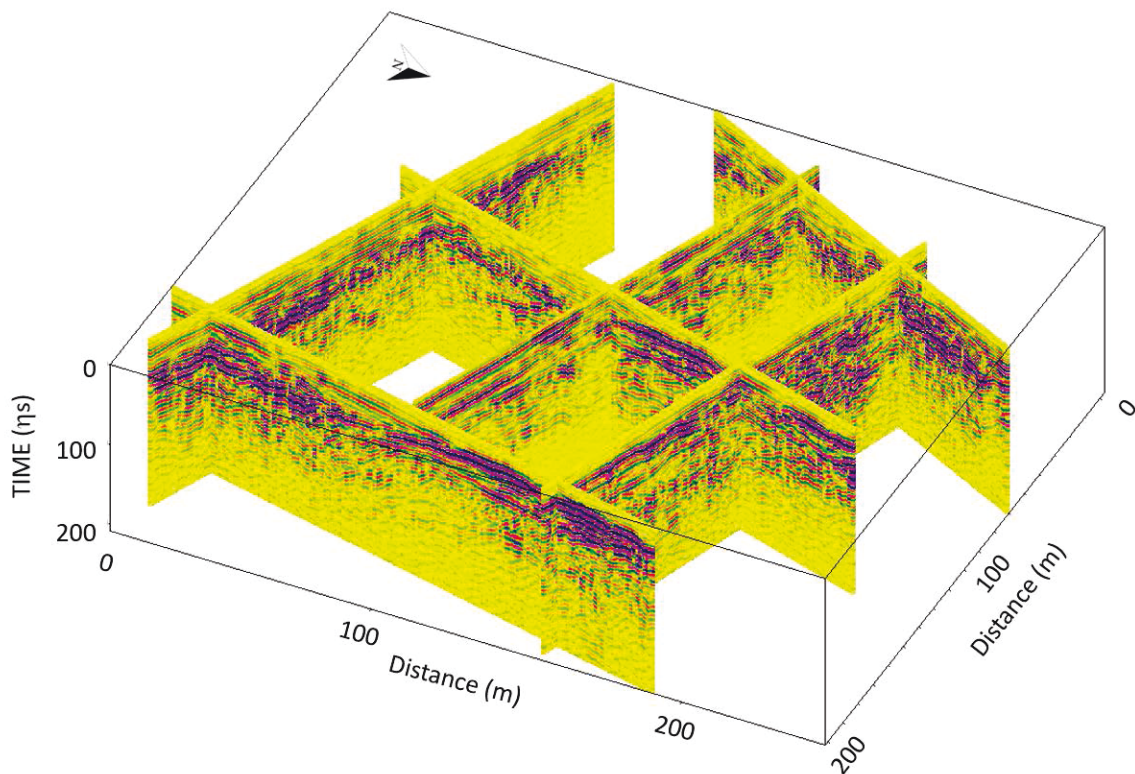


Figure 9. GPR interpreted 3D model.

5 Soil composition

5.1 Grain size distribution

Representative grain size distribution (GSD) curves obtained from OYSB09 samples are presented in Figure 10a. The fine to coarse sandy gravelly soil of Unit I from about 0 m to 10 m depth (mostly classified as well-graded sand (SW after [14]) and the sandy silty layers of soil from Unit II from about 10 m to 20 m depth (classified as silty sand, silt and poorly graded sand (SM, ML and SP after [14]) are represented in this figure. The fines content (particles < 0.06 mm) ranges from 2% to 80%, depending on the soil layer of interest. A classification triangle is given in Figure 10b, showing that the sandy/silty Øysand soils do not contain significant amounts of clay. Fines content is also presented in Figure 13c.

Values of D_{10} and D_{60} are shown in Figure 7f. Values of D_{10} are as low as about 0.02 mm and as high as 1 mm for D_{60} . Higher values of D_{60} and D_{10} are found in the upper layers of Unit I, while lower values are found in Unit II. The variations with depth of the amounts of gravel, sand, silt and clay, by percentage, are shown in Figure 7g. In Unit I,

the gravel content varies between 5% and 50% while the sand content varies between 50% and 90%. In the same unit, the silt content is generally low, usually less than 10% (though some thin layers may have up to 50% silt), and no clay is observed. In Unit II, no gravel content is observed, while the sand contents vary from 25% to 75%. For this same unit, the silt content varies from 25% to 75% while the maximum clay content was below 15% (in the silt layer).

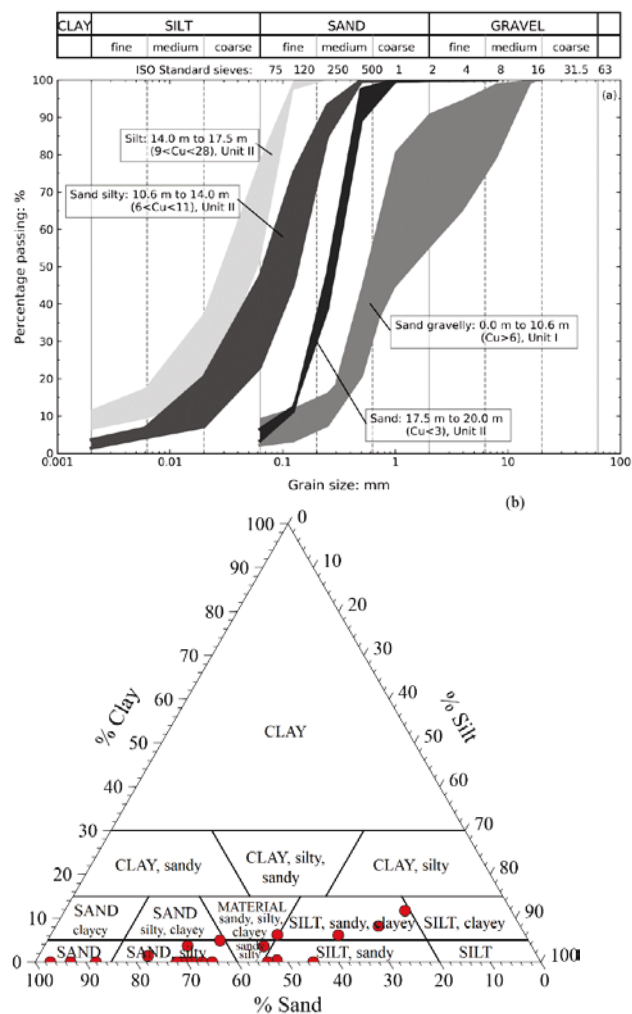


Figure 10. (a) Grain size distributions at Øysand from OYSB09, (b) classification triangle.

5.2 Grain angularity

Particle angularity and sphericity were assessed for gravelly sand samples from 2.5 to 3.6 m depth, using an optical microscope. According to the terminology outlined by [15], Øysand sand particles are mainly sub-rounded and have high sphericity. Detailed results are presented in Table 3. A computed tomography (CT) image from the shallow sand is shown in Figure 11. Note that the grain angularity of the silt layers will be determined in a later stage, using a scanning electron microscope (SEM).

Table 3. Angularity and sphericity (after [15]).

<i>Angularity (from a total of 642 particles observed)</i>						<i>Sphericity</i>	
<i>Very angular</i>	<i>Angular</i>	<i>Sub-angular</i>	<i>Sub-rounded</i>	<i>Rounded</i>	<i>Well-rounded</i>	<i>Low</i>	<i>High</i>
3%	13%	28%	39%	16%	1%	40%	60%

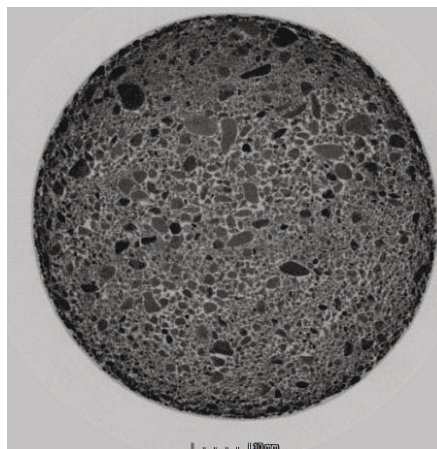


Figure 11. Micro CT scans of shallow gravelly sand 2.5 to 3.6 m depth (from OYSB09).

5.3 Soil fabric

Unit II is generally non-homogeneous, mottled, with primary bedding and laminations depending on the depth of the layer. Micro CT scans of the main types of fabric observed are presented in Figure 12. In Figure 12a a randomly distributed gravelly material in a sandy silty matrix is observed at 14.5 m depth, whereas distinctive layers of gravel and silty sand are shown in Figure 12b at 15.4 m depth. Figure 12c shows the primary inclination of the silty soil from about 16.7 m depth, with typical inclination angles of up to about 25°.

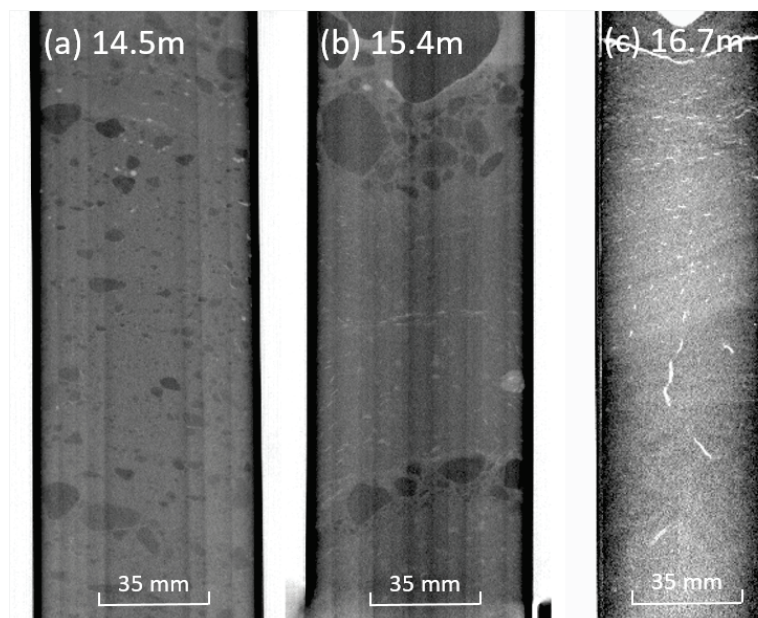


Figure 12. CT-scans of (a) 14.0 m depth, (b) 15.4 m and 16.7 m depth (from OYSB09).

6 Index parameters

6.1 Water content

Water contents, w , were determined using two methods: (i) by oven drying soil samples, and (ii) from multi-sensor core logging. The results summarised in Figure 7 show w increasing from between 10–20% in the unsaturated part of the coarse gravelly sand unit, to values close to 30% in the silty sand of Unit II. Measurements of water content in the gravelly sand layers of Unit I are more scattered than in the samples below 11 m, because water tend to segregate within the tubes towards the bottom of the tube during transportation, handling and storage. MSCL readings are only available from 7.3 m depth and below, results are somehow comparable to the obtained with the method (i). An average of $w = 28\%$ is estimated for Unit II.

6.2 Unit weight of solid particles

Values of the unit weight of solid particles (γ_s), determined according to [16], are shown in Figure 7i.. In Unit I, γ_s varies between 26.5 kN/m³ to 27.2 kN/m³, while in Unit II γ_s is between 26.6 kN/m³ to 26.9 kN/m³. An average value of 26.7 kN/m³ is assumed for Unit II (specific gravity, $G_s = 2.7$).

6.3 Bulk or total unit weight

Total unit weight (γ) was obtained by three different methods: (a) directly from measurements of the weight and volume from piston liners filled with sampled soil, (b) indirectly from water content measurements of the samples and assuming full saturation (reasonable below the ground water level, GWL), and (c) estimated from MSCL readings from 7.2 m to 20 m depth. The unit weight obtained from (a) is less reliable in Unit I soils, because during the sampling process loose material may tend to contract, while dense layers may dilate. As seen in Figure 7e, measurements of γ in the first 7 m depth are quite scattered, low values of unit weight were derived from PPS tubes (between 14 kN/m³ and 17 kN/m³) and high values from water content were obtained (20 kN/m³ to 22 kN/m³). The high variability of unit weight in the upper layers is questioned due to the mentioned sampling issues. In general, the unit weight at OYSB09 ranges between ca. 18 kN/m³ and 20 kN/m³ from 5 m to 20 m depth. A representative profile of 19 kN/m³ can be assumed for the entire site.

6.4 Indirect estimation of in situ relative density

Figure 13a shows the results of $\gamma_{d,max}$ and $\gamma_{d,min}$, obtained using the NGI method [17]. NGI $\gamma_{d,min}$ uses a tube with inner diameter equal 35 mm to place the dry sample in a mould of 72 mm in diameter. As seen in this figure, values of $\gamma_{d,max,NGI}$ and $\gamma_{d,min,NGI}$ change significantly with depth, reflecting the change in particle size distribution at Øysand site. Values of γ_d obtained from γ and the water content as described above are also shown in Figure 13a. Values of D_r determined after four methods are given in Figure 13b, namely a) based on γ_d from the liner tubes, b) from water contents of PPS samples, c) from extruded and trimmed specimens from the PS liners, and d) from CPTU data using [18]. Note that D_r values for the sandy/silty soil from CPTU fall below 40% (from 10 m to 20 m depth), while higher values are determined from the other measurements. For reference, the fines content is also presented in Figure 13c. For depths below 11m depth, the relative density based on water content estimation, or direct measurements of weight and volume from sampled soil is significantly higher than the empirically estimated D_r values using CPTU data. The disturbance induced during the sampling process may have caused the soil to increase its density, hence the values of D_r based on a) b) and c) methods may exceed the *in situ* values. However, D_r estimates derived from CPTU data through calibration chamber tests (such as those reported by [18] on air-pluviated, freshly deposited, uniform, clean (zero fines) normally-consolidated silica sands might also be misleading for the natural Øysand soils. It is estimated that the average relative density of the investigated Øysand soils falls around 60%, with some locally looser soil layers presenting 30% relative density. More exact values of D_r will be acquired from future testing of samples obtained in April and May 2019 by a ground freezing technique.

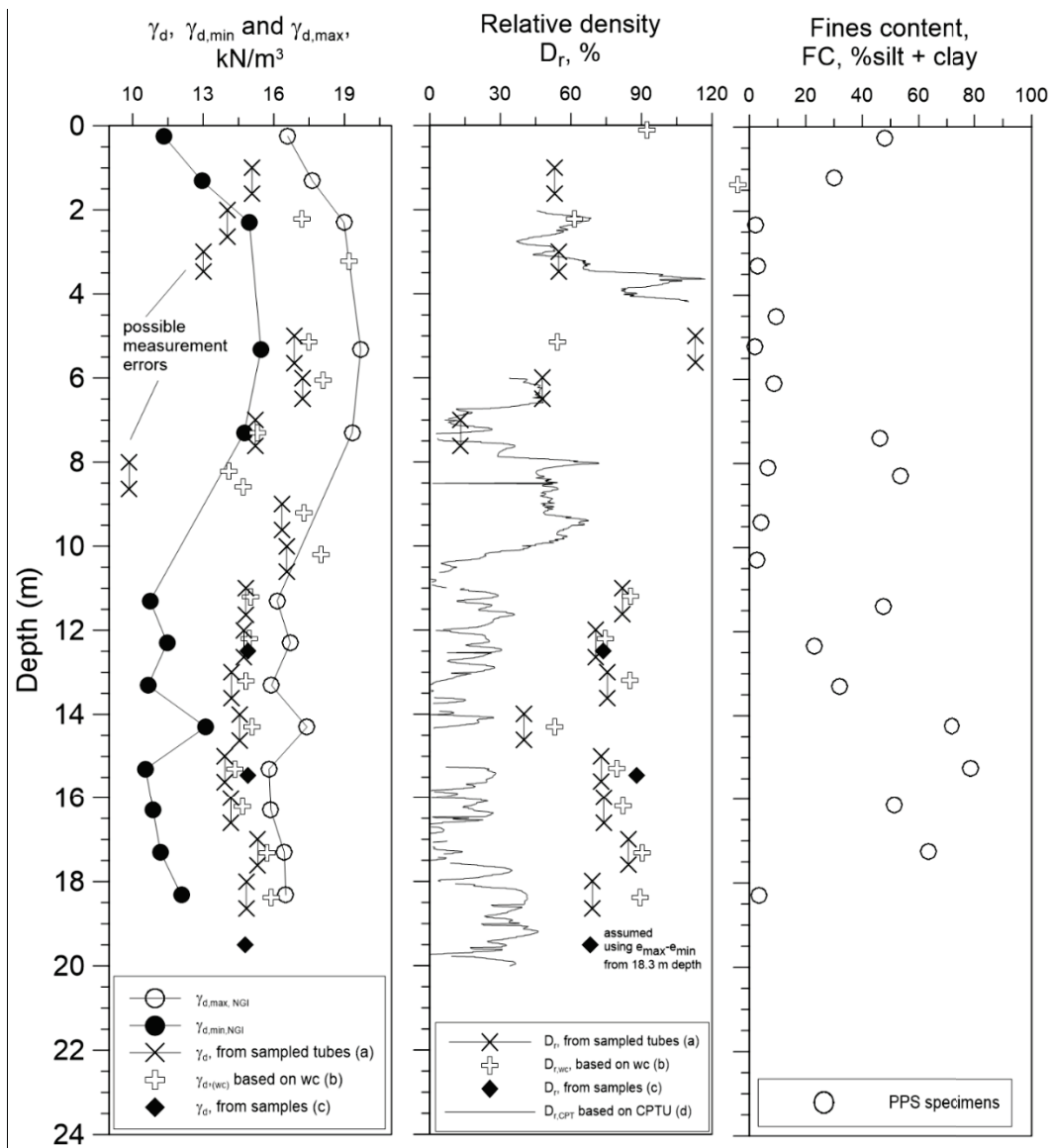


Figure 13. (a) Dry unit weight, maximum and minimum unit weights, (b) relative density, and (c) fines content (from OYSB09).

7 *In situ* testing

Several *in situ* and advanced laboratory tests were performed to determine the engineering parameters of the Øysand site, as listed in Table 1. In this section, the measured *in situ* data is presented first, followed by comparisons of the derived engineering properties from both field and laboratory tests. The presented data focus on the silty sandy materials encountered in Unit II.

7.1 Total sounding (TS)

Total sounding is a static-to-dynamic penetration test method used widely in Scandinavia to determine stratification in soils and to determine the depths to solid ground or bedrock. Test procedures and equipment are described in [19]. The results provide a basis for identifying soils and assessing their relative *in situ* shear strengths, following the procedures described in [19]. Results of all TS tests are summarized in Figure 14. Note that the depths of the TS have been adjusted to focus on the main layers identified across the site. The stiff gravelly layer of variable thickness is observed throughout the site. Hammering and flushing were required to advance through sections of this layer. At locations OYSTS08 and OYSTS09 this layer was mostly penetrable with little hammering, but application of forces in excess of 20 kN was required. At locations OYSTS10 and OYSTS12 similar stiff layers were also encountered. Below this layer softer soils were encountered to at least 20 m depth. The gravelly layers at Øysand are clearly identified when observing Figure 14a. Sandy layers are expected typically below the gravel. Figure 14 provides only an indication of the soil inhomogeneity & variability, and shows qualitatively Unit I (gravelly sand) and Unit II (sandy silty soils).

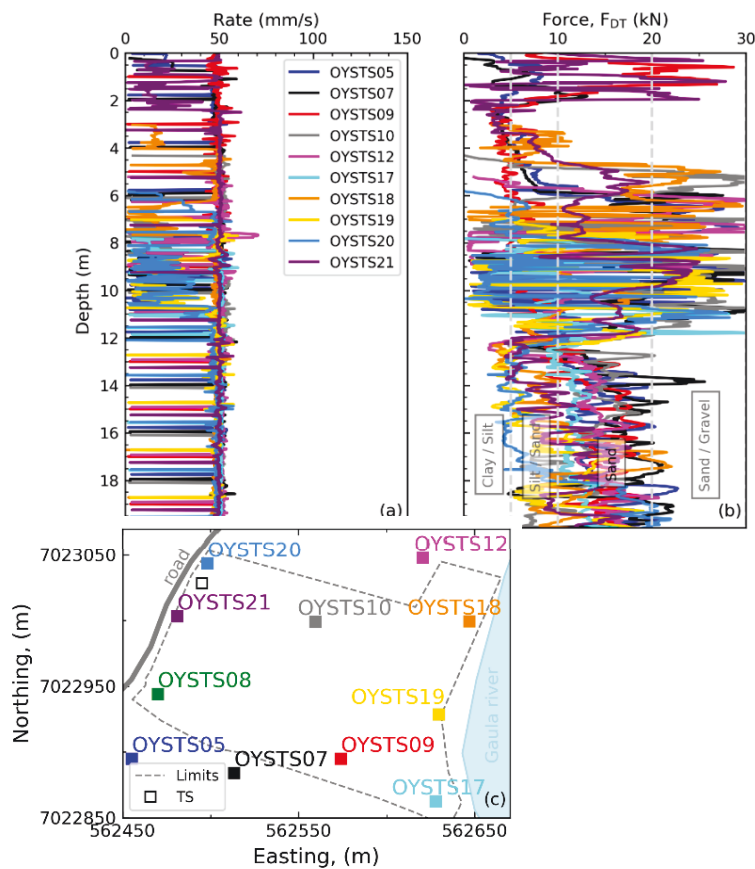


Figure 14. TS tests at Øysand: (a) Drilling rate, (b) force with depth, (c) location plan.

7.2 Cone penetration testing (CPTU)

Figure 15 shows CPTU results in terms of cone resistance, q_c , sleeve friction, f_s , and pore water pressure, u_2 . The CPTU results presented cover the entire area of the site. A Geotech AB CPTU cone was used for the tests shown in Figure 15. CPTU tests employing cones from other manufacturers have also been carried out (see Section 10.1). Testing was performed following [20]. As seen in Figure 15, q_c , f_s , and u_2 measurements vary considerable with depth and location. Most of the CPTU tests were performed from depths below 4 m to avoid damaging the cones on the top gravelly sand layers. Sand layers seem to be thicker at the locations OYSC07, OYSC08, OYSC12, OYSC18 and OYSC20. More silty soils were encountered at locations OYSC02, OYSC10.

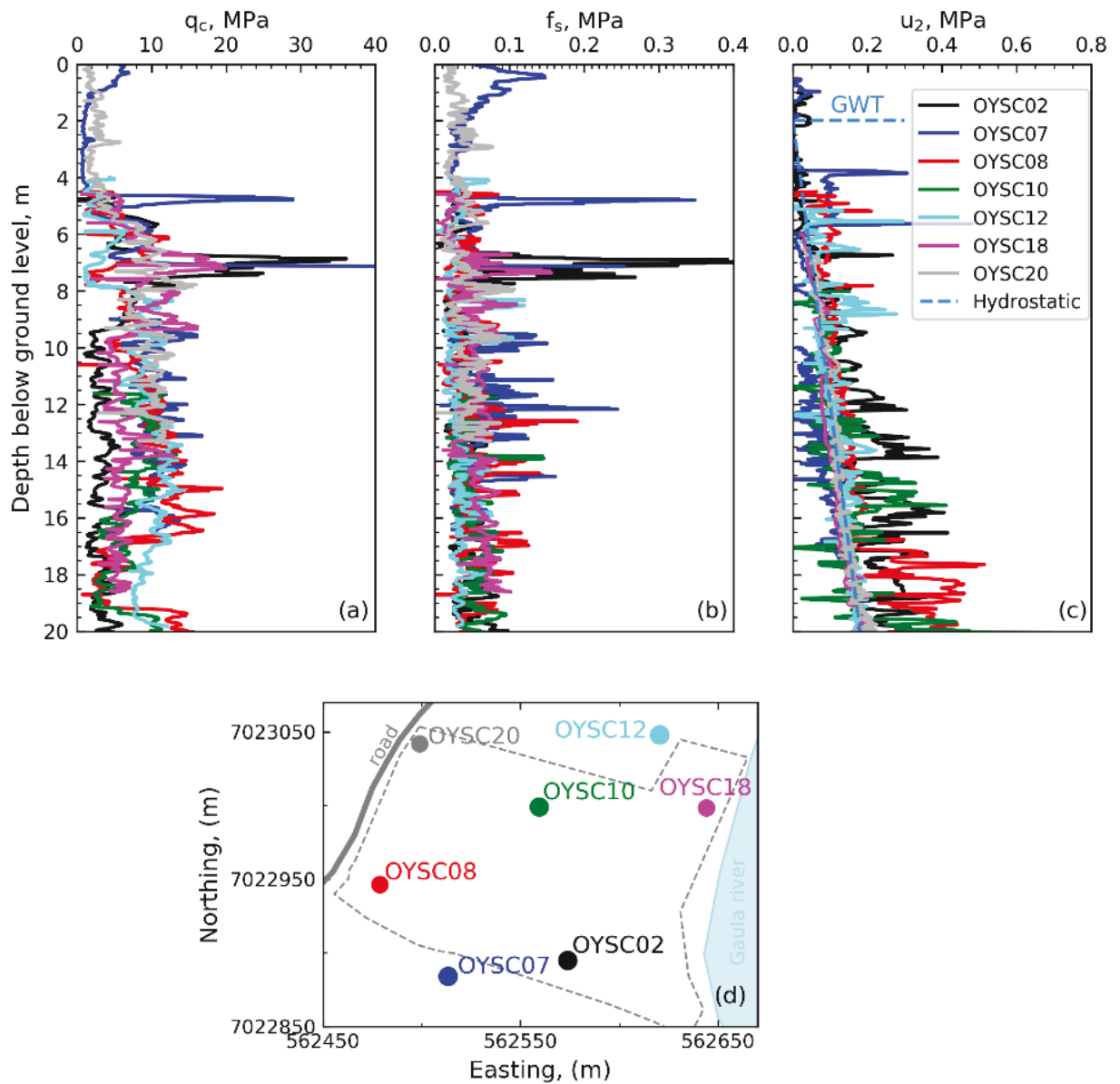


Figure 15. CPTUs around the Øysand site perimeter: (a) q_c (b) f_s , (c) u_2 with depth, and (d) location plan.

The variability of the CPTU data per depth shown in Figure 15, is explained by the depositional history of the site. Unit II consist mostly of deltaic foreset beds dipping at an angle up to 20–25°. There is thus a need for a slight depth adjustment to bring the CPTU data into phase, see Figure 16. The depth-wise correction of the CPTUs helps to visualize the homogeneity of the sand layers across the site.

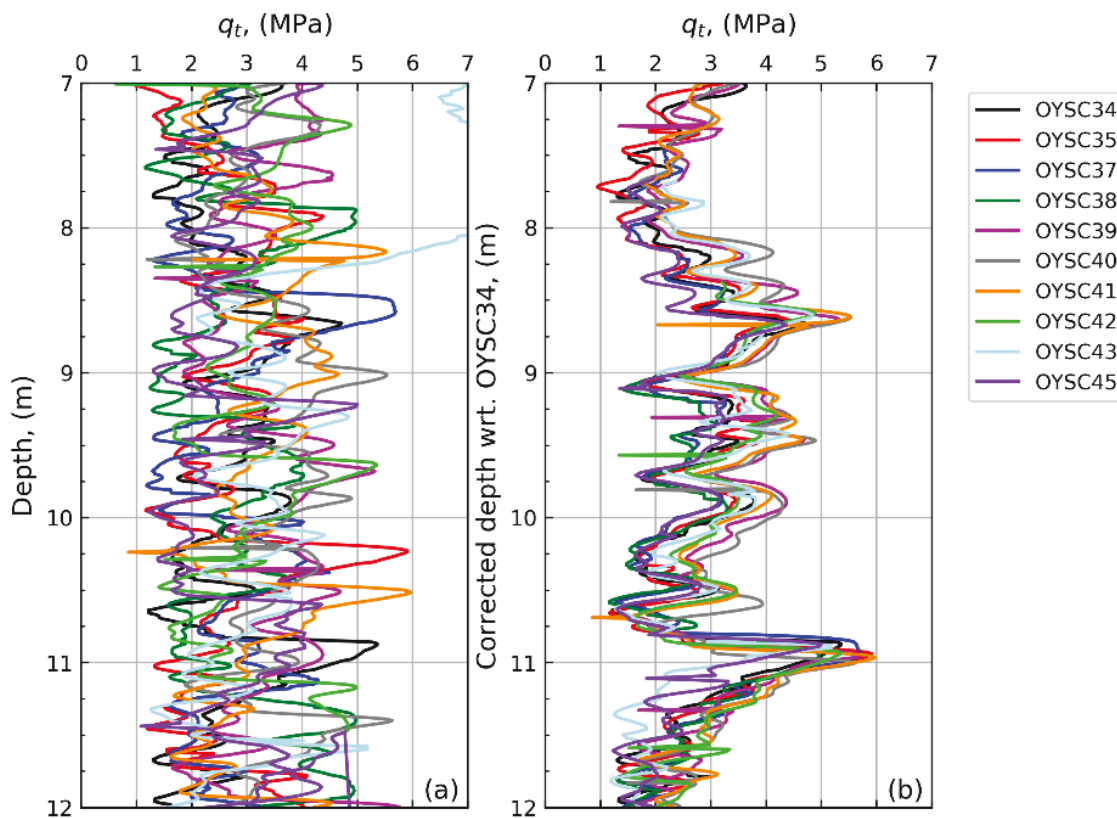


Figure 16. CPTU q_t : (a) uncorrected, (b) corrected depth “in-phase” (modified from [21]).

7.3 Flat dilatometer (DMT)

Two Marchetti SDMT tests (OYSD09 and OYSD18) were performed about 100 m distance from each other. Testing was done by following [22] guidelines. Results are presented in terms of material index, I_D , horizontal stress index, K_D , and dilatometer modulus, E_D , in Figure 17. I_D , K_D and E_D are intermediate parameters, which are obtained from the corrected first and second reading, p_0 , and, p_1 , respectively. In turn p_0 and p_1 are obtained from the DMT readings A and B. Reading A is the pressure required to just begin to move the membrane (lift-off pressure), while reading B is the pressure required to expand the membrane centre 1.1 mm against the soil. Details about the equipment, measurements and test interpretation are found in [23].

As seen in Figure 17, sandy silty soils are indicated as predominating at Øysand, with some locally thick layers of silt towards the south of the site. In general, the DMT measurements are compatible with the stratigraphy described in previous sections. A thorough assessment of the DMT ability to estimate the soil type and unit weight at Øysand is found in [11]. Assessment of OCR and K_0 based on DMT is presented in

Section 9 of this paper.

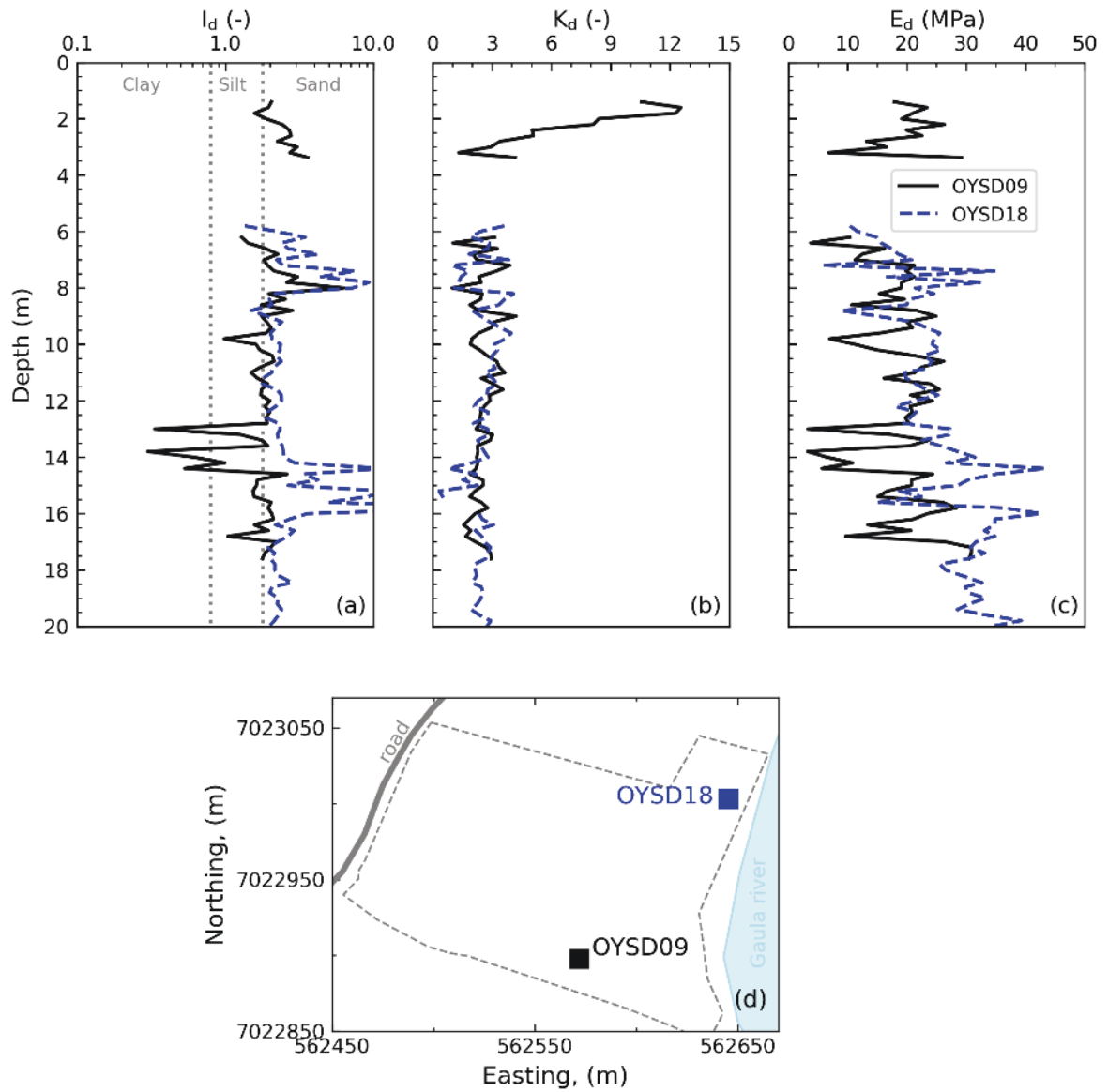


Figure 17. DMT results: (a) Material index, I_D , (b) Horizontal stress index, K_D , and (c) Dilatometer modulus, E_D with depth, and (d) location plan.

7.4 Shear wave velocities (v_s) and small strain stiffness (G_{\max})

Direct measurements of v_s were made using a seismic piezo cone (SCPTU), a seismic dilatometer (SDMT) and MASW. Differences values of v_s can be obtained due to the different propagation and polarization of the waves. In theory, v_s measured with SDMT or SDMT propagate vertically and are horizontally polarized ($v_{s,vh}$), while MASW is closer to $v_{s,hv}$ (horizontally propagating, vertically polarized). Finally, laboratory values of shear waves obtained with bender elements on 54 mm diameter piston samples at NGI, are also presented herein for comparison. Bender element values impose a vertical propagating, horizontal polarized wave $v_{s,vh}$ as SCPTU or SDMT.

MASW (OYSM01 and OYSM03) profiles were acquired at the same locations where SCPTU (OYSC09, OYSC18 and OYSC20) and SDMT (OYSD01 and OYSD02) were performed. As described in [1], the SCPTU or SDMT configurations had a source at ground level and two geophones inside SCPTU, or geophones inside the SDMT, mounted behind the cone or dilatometer, respectively, with a 0.5 or 1.0 m spacing thus giving a measure of $v_{s,vh}$. In order to increase the signal-to-noise ratio on SCPTU readings and reduce the uncoherent noise the seismic traces were typically stacked and filtered through a Butterworth bandpass filter. The velocity was computed from the time lag corresponding to the maximum of the cross-correlation between the two geophone signals. The MASW data acquisition was conducted using a linear array of 24 vertical geophones with a natural frequency of 4.5 Hz, and the inversion of the dispersion curves provided a 1D shear wave velocity, $v_{s,hv}$, profile averaging the subsurface properties below the geophone array.

Parallel tests conducted at locations OYSC09, OYSD01, and OYSM01 allow the various types of measurements to be compared directly. In general, all v_s values vary with the soil layering and depths, as shown in Figure 18. The profile in Figure 18a shows scattered values of $v_{s,SDMT}$ in the upper gravelly sand layers between 0 m and 1 m depth. Measurements of v_s from SCPTU and SDMT do not match well as $v_{s,SCPTU}$ is usually higher than $v_{s,SDMT}$. MASW values of $v_{s,MASW}$ fall in between SCPTU and SDMT results down to about 18 m depth, below that depth MASW results follow the SDMT trend. Note that three different interpretations, by three different engineers, were applied on the MASW data.

Figure 18b shows interpreted G_{\max} values made from the v_s measurements presented in Section 7.4 by assuming unit weights, isotropic elasticity and fixed Poissons ratios. These G_{\max} estimates vary between about 40 MPa and 100 MPa. The scatter of G_{\max} in the gravelly sand of the first 4 m reflects the scatter of v_s measurements and the difficulty of determining γ in those shallow layers. G_{\max} differences between the SCPTU and SDMT derived values naturally follow the same trends as v_s . A significant variation of

G_{max} is observed (± 50 MPa), which is not only attributed to the inherent scatter of the soil, but also to the method used (SCPTU, SDMT, MASW, BE) and geometry of wave polarization. Differences between SDMT and SCPTU can also arise due to the different interpretation methods used while post-processing the data. Moreover, the horizontal and vertical variability of the soil and anisotropy in both fabric and *in situ* stress conditions may generate direction-dependent elastic stiffnesses that also contribute to the discrepancy of the values (see [24, 25]), so that a direct comparison with depth is not strictly possible. Additionally, not all tests were carried out simultaneously, hence changes in the GWL may also lead to small changes in v_s .

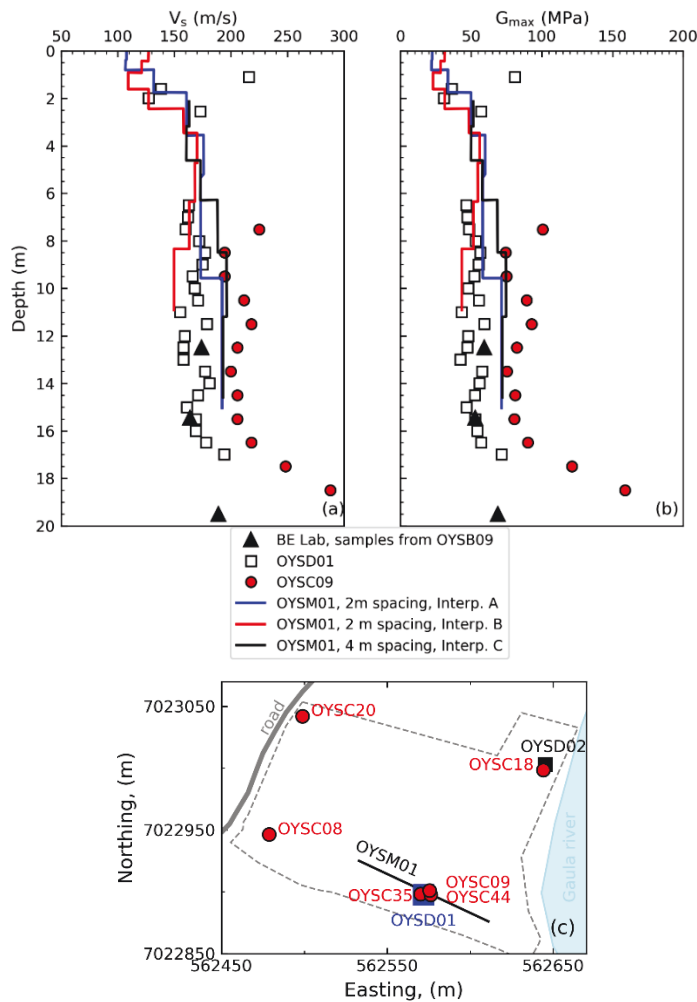


Figure 18. (a) v_s and (b) G_{max} with depth, (c) location plan.

7.5 Permeability (k)

Permeability was assessed by several methods including: (i) slug tests (falling head) on boreholes OYSB04 and OYSB03, (ii) a newly developed permeability cone by NGI [7] at OYSC62 location, (iii) estimates from grain size distribution from soil samples obtained on borehole OYSB09, and (iv) from laboratory tests on 54-mm Geonor push piston samples and on OYSB09 samples. The coordinates of the mentioned locations are shown in Figure 19. As seen in this figure, tests were performed far apart from each other and soil variability probably influenced the results.

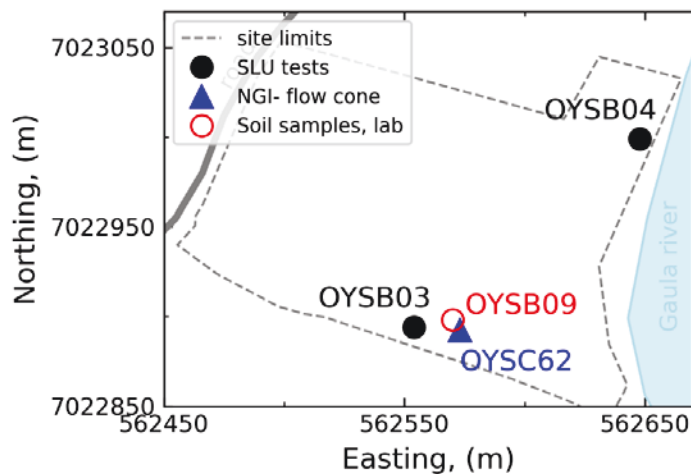


Figure 19. Locations used for permeability assessment.

Nine slug tests were performed in total, 4 on OYSB03 and 5 on OYSB04, in October 2017. A casing was installed in the ground with the use of a sonic drill rig. The top of the casing was 10–20 cm above terrain at the end of the installation. The casing was then filled with water, and the reducing water level inside the casing was logged together with time by a pressure logger installed inside the casing. The air pressure was also logged in order to correct the water pressure measurements. The tests were terminated when the water column inside the casing reached an assumed equilibrium. A sketch of the slug tests, together with the data obtained per depth, are shown in Figure 20. Tests results were assessed using the [26] interpretation procedures.

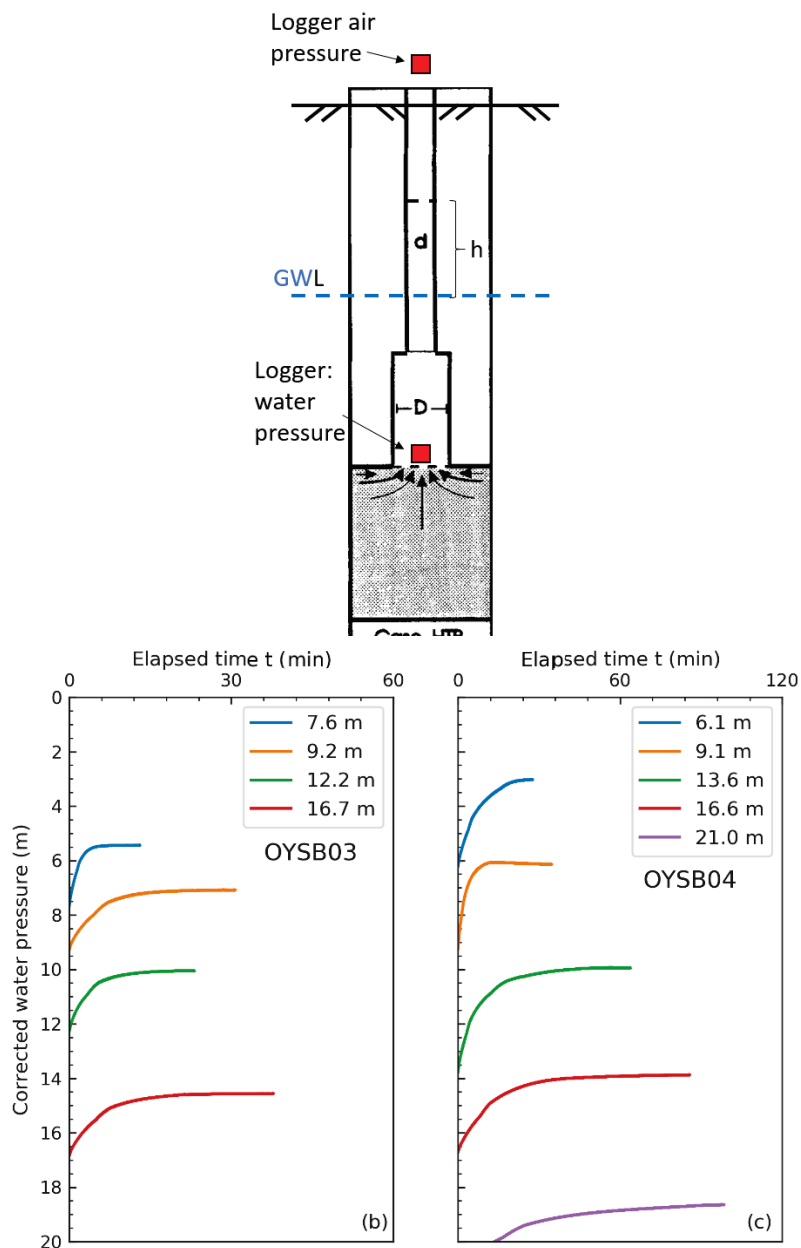


Figure 20. Slug tests: (a) testing scheme (b) tests on OYSB03, and (b) tests on OYSB04.

The NGI permeability flow cone, which has an add-on pumping system that allows water to flow into and out of the surrounding sediments while the CPTU test is performed, was also used at Øysand. Further details on how the flow cone results can be used to estimate the permeability with depth are given in [7].

Permeability estimates were also made based on grain size distribution curves using Hazen’s empirical formulation for saturated sands shown in Eq 1 [27].

$$k = C_H D_{10}^2 \tag{1}$$

where k = permeability (cm/s), C_H = Hazen empirical coefficient, and D_{10} = particle size for which 10% of the soil is finer (cm). C_H was assumed as 100, as is most common in practice; however, values quoted in the literature can range from 1 to 1000. One laboratory constant head test was also conducted during a triaxial test, and slug tests have been carried out in the field. Figure 21 illustrates the cone resistance, soil behaviour type index and hydraulic conductivity from locations OYSC62 (black colour), OYSC60 (OYSB03 – red colour) and OYSC09 (OYSB09 – green colour).

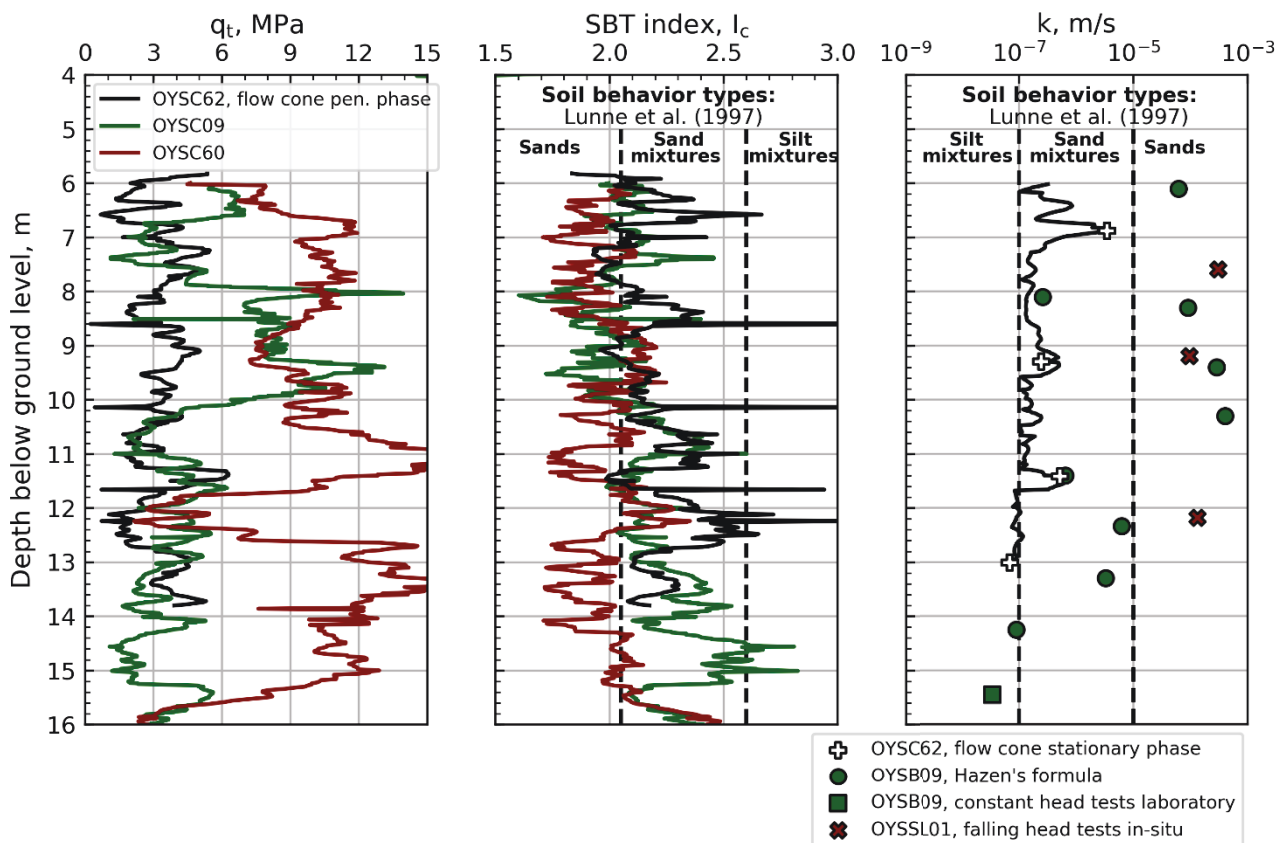


Figure 21. Cone resistance, soil behaviour type index and permeability from [7].

The cone resistance in Figure 21 suggests that there are large variations in soil behaviour for the locations at which the permeability testing was carried out. While the permeabilities from flow cone and Hazen’s formula are comparable at 8 m and 11.4 m depth, there is considerable dispersion over the rest of the entire profile. Hydraulic conductivities from Hazen’s formula generally range between 10^{-7} m/s and 10^{-3} i.e. four orders of magnitude, which may be expected given that the silt content varies between 0 and 70 % (see borehole log in Figure 7). The slug test results generally fall far from the flow cone trends, but are in better agreement with Hazen’s estimation. The differences between the flow cone and slug test results are mainly attributed to different soil conditions at the two test locations. Note that there are uncertainties related to the hydraulic conductivities measured at Øysand, hence the results should be treated with care.

7.6 Soil temperature

Soil temperature was measured between October 2017 and February 2018 (see Figure 22). A fluctuation in the order of about 8°C was observed in the top 8 m of soil. However, below a depth of 8 m, a constant temperature of about 6 degrees Celsius was recorded over the four month period. Knowledge of the temperature of soil layers at the site was important to assess the frost heave susceptibility of Øysand soils and for planning of the soil freezing campaign, which took place during April and May 2019.

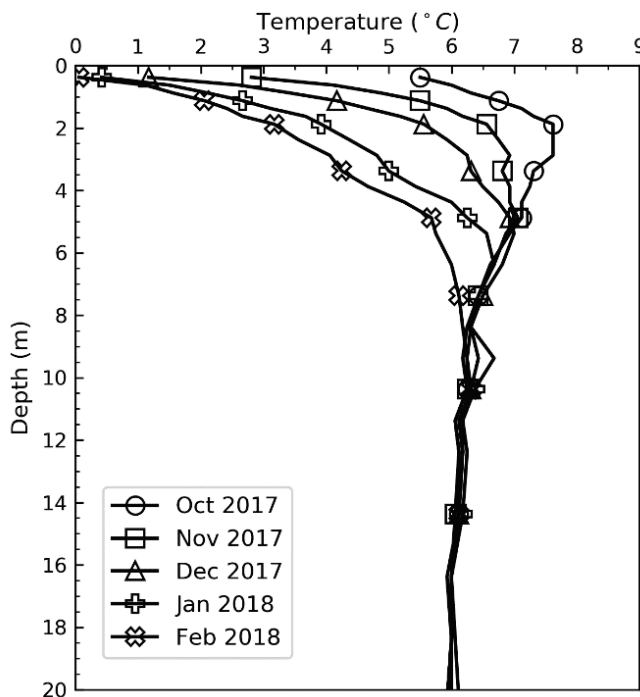


Figure 22. Temperature fluctuations between October 2017 and February 2018.

8 Advanced laboratory testing

8.1 Drained triaxial compression tests

A series of triaxial compression tests were performed on Øysand soil samples obtained with the Geonor push piston sampler at borehole OYSB09. These samples were obtained from the sandy silty soils of Unit II. When the triaxial tests were carried out under anisotropically-consolidated ($K = 0.5$, see Section 9.2) drained compression conditions (CADC), a mainly dilative response was observed. Peak friction angle (ϕ_p) values ranging from 37° to 40° were measured. The large strain angle of shearing resistance (ϕ_{ls}) of the soil tested was equal to about 34° . A plot showing the typical variation of the ratio of deviatoric stress (q) to the mean effective stress (p') with axial strain for three samples collected from different depths is shown in Figure 23.. A comparison between the CADC results obtained so far and correlations for estimating ϕ' found in the literature is presented in Section 9.3.

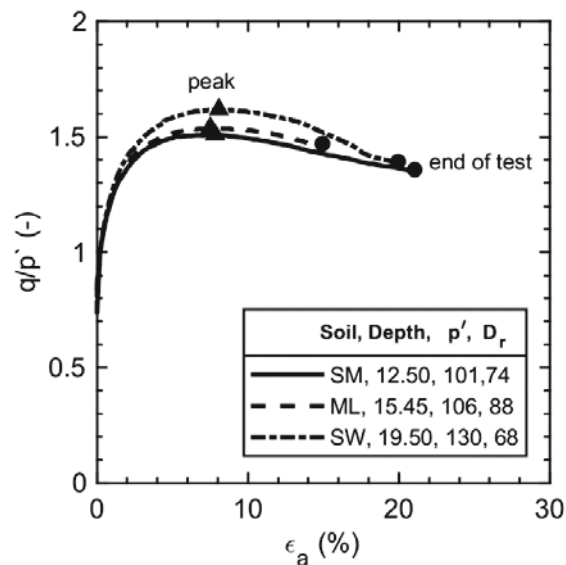


Figure 23. Triaxial test results on Øysand samples from OYSB09.

9 Engineering parameters

9.1 Overconsolidation ratio (OCR)

The overconsolidation ratio, OCR, is defined as the maximum past effective consolidation stress (σ'_p) over the present effective overburden stress (σ'_{vo}). For mechanically overconsolidated soils, where the only change has been the removal of overburden stress, this definition is appropriate. However, for cemented and/or aged soils the OCR may represent the ratio of the yield stress (or apparent overconsolidation) and the present effective overburden stress. Moreover, the yield stress will also depend on the direction and type of loading [28].

Assuming that 7 m of saturated soil was removed at the site by river erosion (groundwater assumed at surface level during erosion, refer to Figure 5), one can estimate the past maximal effective stress, also called the pre-consolidation stress, and OCR. The best estimate of σ'_p and OCR based on the most likely previous terrain level is shown in Figure 24. As shown on this figure, the OCR at about 2 m depth is estimated to be 2.0 and decrease to a value of 1.5 at a depth of 6 m and to a value of 1.2 at 20 m below the ground surface. OCR estimations depend on the assumption made with respect to the groundwater level during the erosion process.

OCR was estimated from CPTU tests using [29] unified-approach for evaluation of the yield stress. The equation presented by them is given below and it is considered as first-order estimation of the yield stress:

$$\sigma'_p = 0.33(q_t - \sigma_{vo})^{m'} \quad (2)$$

where, σ'_p = past effective consolidation stress, q_t = corrected cone resistance ($q_t = q_c + u_2(1 - a)$) in kPa, σ_{vo} = vertical total stress in kPa, and m' is the fitting exponent = $m' \approx 0.72$ for clean quartz to silica sand, 0.8 in silty sands, 0.85 in silts, 0.90 in organic and sensitive fine-grained soils, and $m = 1.0$ in intact clays of low sensitivity.

OCR profiles based on the [29] equation are shown in Figure 24. The Øysand site is classified as normally consolidated (NC) or slightly overconsolidated (OC). Assuming an overburden pressure of 7 m of soil for calculating σ'_p can be used for calculating an upper boundary of OCR (see dashed lines profile in Figure 24).

Marchetti (1980) proposed the empirical equation $OCR_{DMT} = (0.5 K_D)^{1.56}$ for estimating OCR (and K_0) of NC-clays or soils of $I_D < 1.2$ (Øysand sand has shown I_D values below about 2). There have been several other attempts for obtaining OCR-DMT correlations, e.g. [30–32]. However, according to [33], such correlations have been reported to be only of local applicability. According to [34], the estimation and the definition of OCR in sands

is more difficult and a combination of CPT and DMT readings (M_{DMT}/q_c) may be the only way of obtaining an idea of OCR in sands. The following empirical correlation for Venice lagoon was proposed by [33].

$$OCR = 0.0344(M_{DMT}/q_c)^2 - 0.4174(M_{DMT}/q_c) + 2.2914 \quad (3)$$

where, M_{DMT} = constrained modulus, calculated by $M_{DMT} = R_M E_D$, and $R_M = f(I_D, K_D)$.

OCR results based on combined CPTU and DMT readings are plotted in Figure 24. Those OCR values fit with OCR estimated from CPTU tests.

9.2 Coefficient of earth pressure at rest, K_0 , and estimated in situ effective stresses

The coefficient of lateral earth pressure at rest is defined as:

$$K_0 = \frac{\sigma'_{ho}}{\sigma'_{vo}} \quad (4)$$

where, σ'_{ho} = effective horizontal stress and σ'_{vo} = effective vertical stress. Typical values of K_0 reported in the literature are 0.5 for NC sands and 1.0 for OC sands.

Based on the simplified equation by [35, 36] and to reflect the effect of OCR on K_0 , a variation of K_0 has been proposed by [37]:

$$K_0 = (1 - \sin\phi)OCR^{\sin\phi} \quad (5)$$

where ϕ is assumed to be ϕ'_{cv} (the constant-volume effective stress friction angle), as proposed by [38] based on oedometer test on dense and loose sand. A value of $\phi'_{cv} = 30^\circ$ has been assumed for Øysand site. K_0 values based on CPTU tests have been obtained using Eq 5, and OCR based on [32], results are show in Figure 24.

A multi-parameter approach similar to the OCR estimation has been proposed by [31] for calculating K_0 from CPT and DMT tests based on the calibration chamber data from [39] for Ticino and Hokksund sands. The equation for calculating K_0 is

$$K_0 = 0.376 + 0.095K_D - D_3 \left(\frac{q_c}{\sigma'_v} \right) \quad (6)$$

where D_3 = fitting parameter reported to be 0.0017 for calibration chamber data obtained from pluviated sand or 0.0046, which is a modified parameter to predict K_0 for the natural Po river sand. D_3 coefficient can be assumed to be 0.005 in sand deposited hundreds to thousands of years previously and 0.002 in freshly deposited sand [39]. A

value of 0.005 was used to calculate the values of K_0 presented in Figure 24. The representative profile of K_0 , based on a past overburden pressure of 7 m of soil is also shown in dashed lines on that figure.

Figure 24c shows profiles of water pressure (u_w , based on piezometric data), $\sigma_{tot,v}$ calculated from the unit weight values presented in Figure 7, σ'_v and σ'_h using the estimated K_0 values estimated from Figure 24b. Note that OCR and K_0 are not fixed values, they change with varying effective stresses, e.g. during seasonal variations of the groundwater as shown in Figure 4.

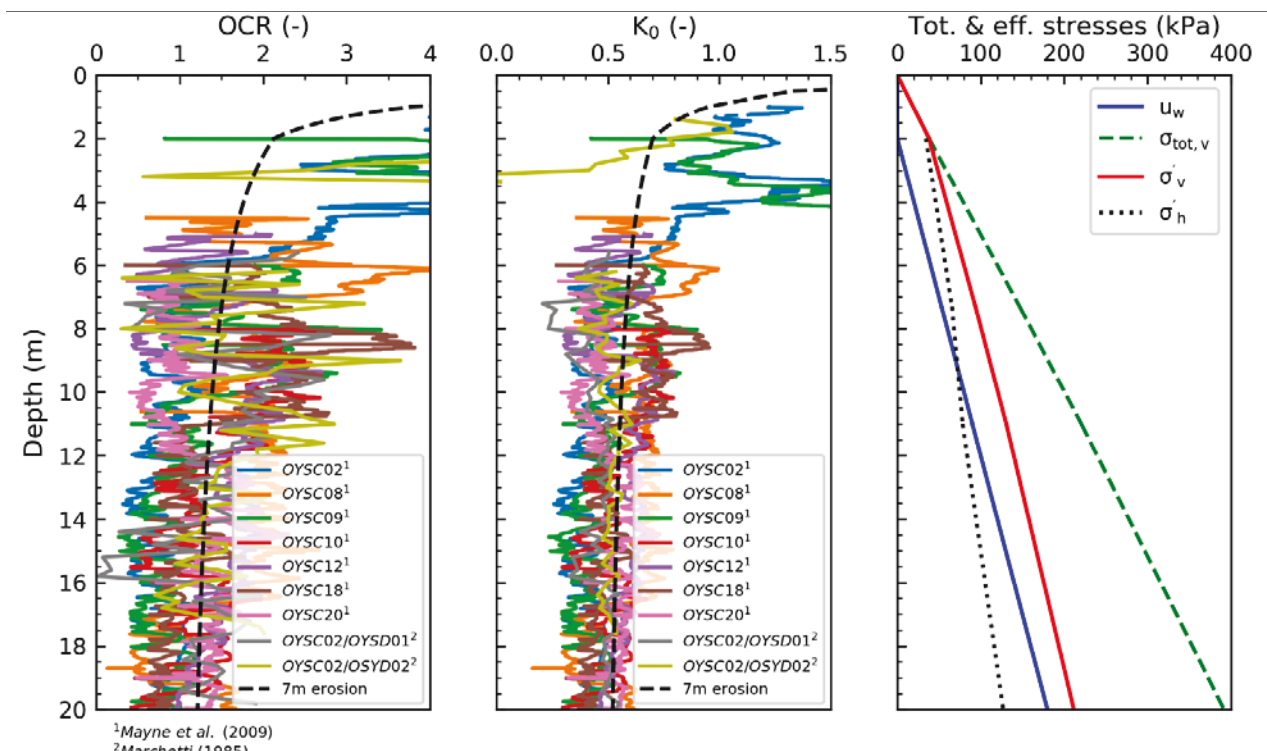


Figure 24. Estimation of: (a) OCR, (b) K_0 , and effective stresses with depth.

9.3 Effective stress-strength parameters—field and laboratory testing

The peak and large strain angle of shearing resistance obtained from anisotropically consolidated drained (ϕ_p , ϕ_{ls}) triaxial compression tests (CADC) are compared against values estimated from empirical correlations from field tests available in the literature. CPTU, DMT and v_s were used to estimate *in situ* friction angles.

For estimating the angle of shearing resistance based on CPTU data, the relationship

between normalized cone resistance, Q_t and ϕ'_p after [40] was chosen, see Eq 7. The relationship is valid for uncemented, unaged, freshly deposited sand, moderately compressible, predominately quartz sands.

$$\phi'_{p,CPT} = 17.7^\circ + 11.0^\circ \times \log(q_{t1}) \quad (7)$$

where, q_{t1} = normalized cone resistance ($q_{t1} = q_t / (p_a \cdot \sigma'_{vo})^{0.5}$).

An equation for estimating a so-called safe (or lower bound) angle of shearing resistance, $\phi_{safe,DMT}$ based on DMT data has been proposed by [41]. The equation is valid for unaged, uncemented sands. $\phi_{safe,DMT}$ is calculated from the intermediate parameter K_D , see Eq 8.

$$\phi'_{safe,DMT} = 28 + 14.6 \log(K_D) - 2.1 \log(K_D)^2 \quad (8)$$

where, K_D = Horizontal stress index ($K_D = (p_0 - u_0) / \sigma'_{vo}$), p_0 = DMT first correct reading.

Since v_s is more sensitive to OCR, D_r and the sand's microstructural features, e.g. cementation, bonding and ageing, an estimation of ϕ_p from v_s was made. The following correlation for estimating of ϕ'_p on sands based on v_{s1} has been proposed by [42].

$$\phi_{p,v_{s1}} = 3.9(v_{s1})^{0.44} \quad (9)$$

where, ϕ_p = peak friction angle and v_{s1} = normalized shear wave velocity ($v_{s1} = v_s / (p_a / \sigma'_{vo})^{0.25}$), p_a = atmospheric pressure = 100 kPa, and σ'_{vo} = vertical effective stress.

Estimated values of peak friction angle based on CPTU, DMT and v_s , in comparison with laboratory data from CADC tests, are shown in Figure 25. In general, reasonable estimations of ϕ'_p based on CPTU and v_s were obtained. The DMT correlation estimates ϕ'_{safe} values, somewhat lower than the measured $\phi'_{ls} = 34^\circ$ from triaxial tests. Note that peak friction angles depend on the sand state, which may have been affected by the sampling process. Hence, the currently presented laboratory values of ϕ'_p should be taken with care. The level of disturbance of samples obtained with a piston sampler can be significant in sands.

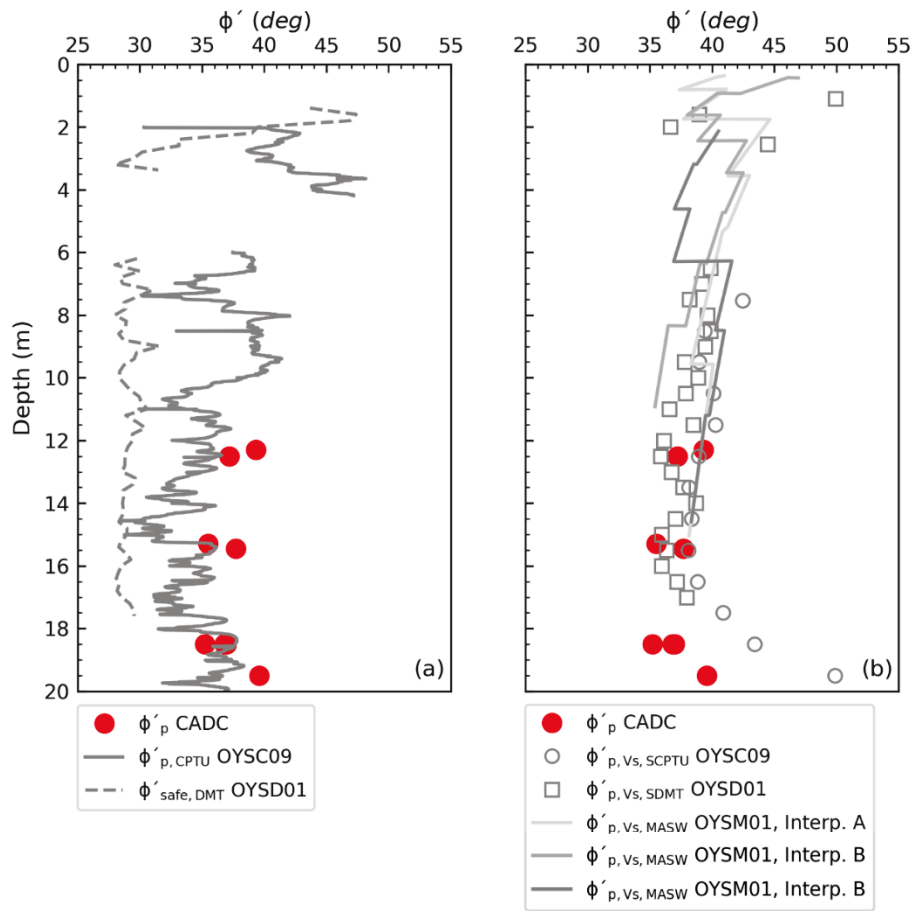


Figure 25. Variation of friction angles from drained triaxial tests on samples from OYB09 with depth.

10 Further geotechnical characterisation considerations

10.1 Impact of cone penetrometer type on CPTU results

CPTUs from several manufacturers were tested at Øysand, including Geomil, A.P.van den Berg, Pagani, Environmental Mechanics (Envi) and Geotech AB CPTU cones. The 7 cones types used are 10 cm² compression cones with 150 cm² friction sleeves and the pore pressure transducer located in the u₂ position. The CPTU tests were carried out following [20]. CPTUs were performed very close to each other, to avoid as much as possible the inherent soil variability. Results of different cones types are presented in Figure 26. Details of the cones type used (geometry, calibrations, filter materials, saturation fluids used, etc.) are found in [43]. As seen in Figure 26, q_t can vary about 2 MPa, f_s up to 0.08 MPa and u₂ up to 0.2 MPa depending on the CPTU type used. In general, the smallest variability is observed for u₂. Hence, u₂ is the most reliable parameter. The largest variation is observed in f_s, making this parameter the least reliable. The research showed also the importance of good procedures for taking zero readings and also taking into account temperature effects on CPTU readings.

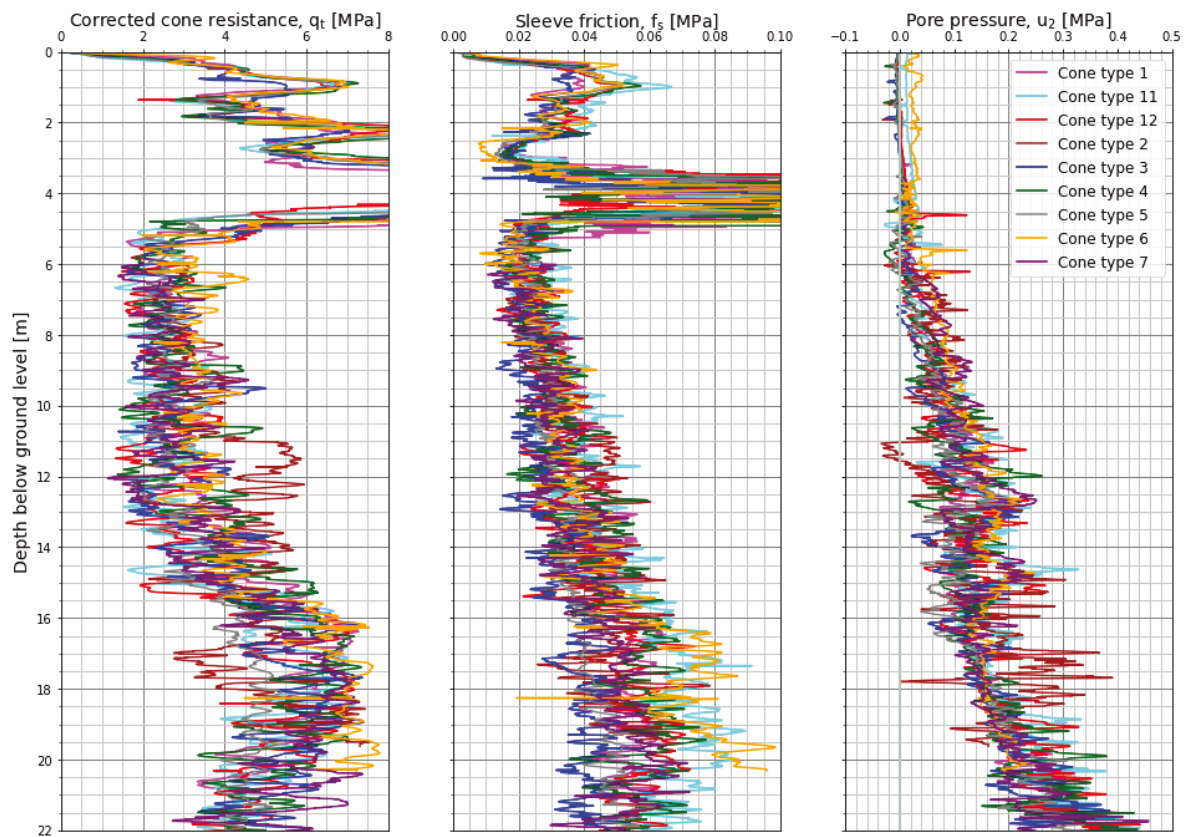


Figure 26. Variation of CPTU readings depending on cone type: (a) q_c , (b) f_s , (c) u_2 with depth.

10.2 Sample quality research in progress

An evaluation of sample quality is ongoing for the Øysand site. As described in Table 1 soil sampling has been and will be done using several techniques. Those techniques are: (i) Geonor 54 mm fixed piston composite sampler, (ii) 72 mm thin walled fixed piston sampler, (iii) Gel-Push sampler (without success so far, only two samples obtained) and (iv) soil freezing (see Figure 27). Results from the ground freezing investigation are in progress and will be reported subsequently. Reconstituted specimens will also be tested, and the results of “intact” and reconstituted advanced tests will be compared.



Figure 27. Installation of soil freezing pipes at Øysand in March 2019.

10.3 Frost heave susceptibility of Unit II sandy/silty soils

Since a ground freezing campaign is being performed at Øysand, it was necessary to assess the frost susceptibility of the soils to be frozen. Sandy silty mixtures at Øysand are classified as frost susceptible. The main Øysand soil types will be tested in the one-dimensional freezing cell to determine if they are susceptible to heave expansion. The cell used was developed by the Korean Institute of Civil Engineering and Building Technology (KICT) and modified at NGI. Details of the cell development and its components are found in [44]. An image of the modified setup used is shown in Figure 28. Preliminary results have shown that sandy soil layers at Øysand are not frost susceptible, hence the ground freezing technique can be used for stabilization prior to

sampling of those soils.

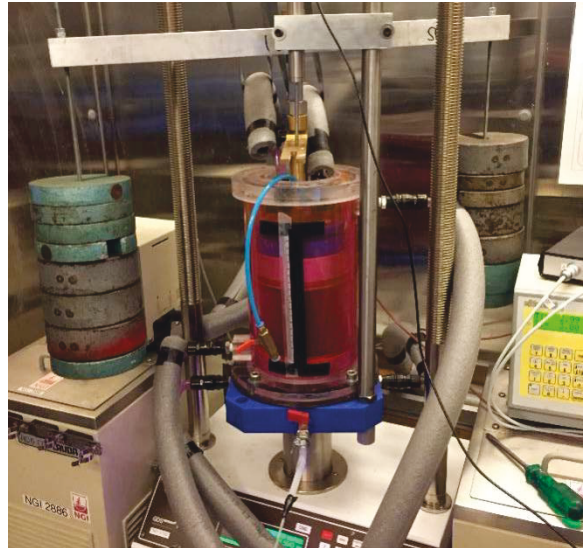


Figure 28. Frost susceptibility test on Øysand soils.

11 Summary and conclusions

This paper presents an overview of the geophysical and geotechnical characterisation of the sandy silty soils of the Øysand research site. State-of-the-practice and state-of-the-art *in situ* characterisation techniques have been used to investigate stratigraphy and to derive engineering parameters. Shear strength and stiffness parameters have been presented from both *in situ* and laboratory testing approaches. Examples of engineering characterisation problems currently being investigated at Øysand have also been discussed. Insights obtained so far include:

- The fluvial and deltaic deposits encountered show lateral (mainly north to south) and vertical variations. The main layers identified comprise: a gravelly sand layer encountered down to a maximum of 10 m depth over sandy silty soils that were proven down to 20 m depth. The bedrock depth was not established, but is thought to exceed 80 m.
- Comprehensive field and laboratory testing programmes have been carried out on the site. The geotechnical tools include total sounding, seismic penetrometer, piezometer, seismic dilatometer, multi-channel analysis of surface waves, slug tests and temperature measurements. Laboratory testing include index and advanced laboratory testing.
- The Øysand site soils are normally-to-lightly overconsolidated; the large strain angle shearing resistance of the sand layer at OYSB09 is equal to about 34°. A

strongly dilative response was observed during drained laboratory triaxial compression tests on tubed 54 mm diameter Geonor push piston samples. Peak angles of shearing resistance of up to 40° were measured in these tests. G_{\max} values varied between about 50 MPa and 100 MPa depending on the *in situ* tool used and depth. Soil permeability measurements ranged over several orders of magnitude. The determination of k is highly method dependent. At Øysand, permeability ranges between 10^{-7} m/s and 10^{-3} m/s. Temperature fluctuations of the upper 8 m have been recorded. Below that depth, a constant temperature of 6°C is observed.

- Some geotechnical engineering characterisation problems under investigation at Øysand have been briefly introduced. Those problems are related to (i) the impact of using different CPTU types, (ii) the assessment of sample quality by sampling soil using different state-of-the-practice and state-of-the-art techniques, and (iii) determining the frost susceptibility of Øysand soils.

Acknowledgments

The authors would like to thank Tom Lunne for his support and the Research Council of Norway for their generous infrastructure grant to establish the five Norwegian GeoTest Sites for research (Grant No. 245650/F50). The authors acknowledge the significant contributions from Pagani, Geomil Equipment, In situ SI, the Norwegian Public Roads Administration, Geological Survey of Norway and colleagues at NGI Field Investigations (Kristoffer Kåsin, Pål Kristian Karstensen, Magnus Hunemo, Rolf Ove Karlsen and Håvard Saur) and NGI Geosurveys (Helge Smebye and Sara Bazin). The work presented in this paper is part of the PhD research of the leading author at Imperial College London, funded by the Norwegian Geotechnical Institute and the Norwegian Research Council.

Conflict of Interest

All authors declare no conflicts of interest in this paper.

References

1. L'Heureux JS, Lunne T, Lacasse S, et al (2017) Norway's National GeoTest Site Research Infrastructure (NGTS). In: Proceedings of the 19th International Conference on Soil Mechanics and Geotechnical Engineering. Seoul
2. Blaker Ø, Carroll R, Paniagua P, et al (2019) Halden research site: geotechnical characterization of a post glacial silt. AIMS Geosci 5:184–234
3. Gundersen AS, Hansen RC, Lunne T, et al (2019) Characterization and engineering properties of the NGTS Onsøy soft clay site. AIMS Geosci 5:665–703
4. L'Heureux JS, Lindgård A, Emdal A (2019) The Tiller-Flotten research site: Geotechnical characterization of a very sensitive clay deposit. in press
5. Gilbert GL, Instanes A, Sinitsyn AO, Aalberg A (2019) Characterization of the NGTS permafrost sites: Longyearbyen, Svalbard. in press
6. Salgado R (2008) The engineering of foundations. McGraw-Hill New York
7. Gundersen AS, Lunne T, Carotenuto P, et al (2019) Measurements of hydraulic soil properties at NGTS sand site using a newly-developed in-situ tool. in press
8. Reite AJ (1994) Weischelian and Holocene geology of Sør-Trøndelag and adjacent parts of Nord-Trøndelag county, Central Norway. Norges Geol undersøkelse-Bulletin 1–30
9. Reite AJ, Sveian H, Erichsen E (1999) Trondheim fra istid til nåtid – landskapshistorie og løsmasser. Norges Geol undersøkelse Gråsteinen 5:40 p.
10. Wolff FC (1979) Beskrivelse til de berggrunnsgeologiske kart Trondheim og Østersund 1:250 000. Norges Geol undersøkelse 353:76
11. Gundersen AS, Quinteros S, Heureux JSL, Lunne T (2018) Soil classification of NGTS sand site (Øysand , Norway) based on CPTU , DMT and laboratory results. In: 4th International Symposium on Cone Penetration Testing. CPT18. pp 323–328
12. Cosentini RM, Della Vecchia A G, Foti S, Musso G (2012) Estimation of the hydraulic parameters of unsaturated samples by electrical resistivity tomography. Géotechnique 62:583–594
13. Lunne T, Robertson PK, Powell JJM (1997) Cone Penetration Testing in Geotechnical Practice. New York
14. ASTM (2017) D2487 - 17 Standard Practice for Classification of Soils for Engineering Purposes (Unified Soil Classification System)
15. Powers MC (1953) A new roundness scale for sedimentary particles. J Sediment Petrol 117–119
16. NS 8012 (1982) Geoteknisk prøving. Laboriemetoder. Korndensitet. Standard Norge, Lysaker.
17. Lunne T, Knudsen S, Blaker Ø, et al (2019) Methods used to determine maximum and minimum dry unit weight of sand. Is there a need for a new standard? Can Geotech J 56:536–553
18. Jamiolkowski M, Lo Presti DCF, Manassero M (2003) Evaluation of relative density and shear strength of sands from CPT and DMT. In: Germaine JT,

- Sheahan TC, Whitman RV (eds) Soil behavior and soft ground construction. ASCE GSP, pp 201–238
19. NGF (2018) Guidelines for performing total sounding tests (In Norwegian: Veiledning for utførelse av totalsondering). Norwegian Geotechnical Society, Norway
 20. ISO 22476-1 (2012) Geotechnical investigation and testing - Field testing - Part 1: Electrical cone and piezocone penetration test
 21. Liu Z, Wist Amdal ÅM, L'Heureux JS, et al (2019) Spatial variability of medium dense sand deposit. in press
 22. ISO 22476-11 (2017) Geotechnical investigation and testing - Field testing - Part 11: Flat dilatometer test
 23. Marchetti S (1980) In situ tests by flat dilatometer. J Geotech Eng Div ASCE 106:299–321
 24. Kuwano R, Jardine RJ (2002) On the applicability of cross-anisotropic elasticity to granular materials at very small strains. Geotechnique 52:727–750
 25. Jardine RJ (2013) Advanced laboratory testing in research and practice. . 2nd Bishop Lecture. In: Delage et al. (ed) Proc. ICSMGE. Presses des Ponts, Paris, p Vol 1, pp. 35–55
 26. Demir Z, N. Narasimhan T (1994) Improved Interpretation of Hvorslev Tests. J Hydraul Eng 120:477–494
 27. Hazen A (1911) Discussion of Dams on sand foundations. transactions Am Soc Civ Eng 73:199–203
 28. Robertson PK, Cabal KL (2015) Guide to Cone Penetration Testing for Geotechnical Engineering, 6th Editio. Gregg Drilling & Testing Inc., California
 29. Mayne PW (2009) Geoengineering Design Using the Cone Penetration Test. ConeTec Inc., Richmond, BC, Canada
 30. Schmertmann JH (1983) Revised procedure for calculating K_0 and OCR from DMT's with $I_d > 1.2$ and which incorporates the penetration force measurement to permit calculating the plane strain friction angle. In: Proc. of the 1st Int. Conf. on the Flat Dilatometer. Gainesville, FL.
 31. Marchetti S (1985) On the field determination of K_0 in sand. In: 11th Int. Conf. on Soil Mech. and Found. Eng. Panel Presentation, Balkema Pub., Rotterdam, p Vol. 5, pp. 2667–2672
 32. Mayne P, R Coop M, Springman S, et al (2009) Geomaterial behavior and testing. In: Hamza M, Shahien, M.El-Mossallamy Y (eds) Proc. 17th International Conference on Soil Mechanics and Geotechnical Engineering. Alexandria, Egypt, pp 4:1-96
 33. Monaco P, Amoroso S, Marchetti S, et al (2014) Overconsolidation and Stiffness of Venice Lagoon Sands and Silts from SDMT and CPTU
 34. Marchetti S, Monaco P, Totani G, Calabrese M (2001) The Flat Dilatometer Test (DMT) in Soil Investigations
 35. Jaky J (1944) The coefficient of earth pressure at rest. In Hungarian (A nyugalmi nyomas tenyezoe). J Soc Hung Eng Arch (MagyarMernok es Epit Kozlonye) 355–358

36. Jaky J (1948) Pressure in silos. In: Proc. 2nd Int. Conf. on Soil Mechanics and Foundation Engineering. Rotterdam, The Netherland, pp 1:103-10
37. Mayne P, Kulhawy FH (1982) Ko – OCR relationships in soil. J Geotech Eng Div ASCE 108:851–872
38. Lee J, D. P, Kyung D, Lee D (2003) Effect of particle characteristics on Ko behaviour of granular materials. In: Proceedings of the 18th International Conference on Soil Mechanics and Geotechnical Engineering. September 2-6, Paris, pp 337–380
39. Baldi G, Bellotti R, Ghionna V, et al (1986) Interpretation of CPTs and CPTUs; 2nd part: drained penetration of sands. In: Proceedings of the Fourth International Geotechnical Seminar. Singapore, pp 143–156
40. Mayne PW (2014) KN2: Interpretation of geotechnical parameters from seismic piezocone tests. In: Robertson PK, Cabal KL (eds) Proceedings, 3rd International Symposium on Cone Penetration Testing (CPT'14, Las Vegas). ISSMGE Technical Committee TC 102, pp 47–73
41. Marchetti S (1997) The Flat Dilatometer: Design Applications. In: Third Geotechnical Engineering Conference Cairo University. Cairo, pp 421–448
42. Uzielli M, Mayne P, Cassidy M (2013) Probabilistic assignment of design strength for sands from in-situ testing data. In: Advances in Soil Mechanics & Geotechnical Engineering (series), Vol. 1. IOS-Millpress, Amsterdam, pp 214–227
43. NGI (2018) Impact of cone penetrometer type on CPTU results at 4 NGTS Sites. Silt, Soft Clay, Sand, and Quick Clay. Report No. 20160154-21-R. Oslo, Norway
44. Jin HW, Lee J, Ryu BH, Akagawa S (2019) Simple frost heave testing method using a temperature-controllable cell. Cold Reg Sci Technol 157:119–132

**AIMS Geosciences**

© 2019 the Author(s), licensee AIMS Press. This is an open access article distributed under the terms of the Creative Commons Attribution License

(<http://creativecommons.org/licenses/by/4.0>)



Dokumentinformasjon/Document information		
Dokumenttittel/Document title Øysand research site: Geotechnical characterisation of deltaic sandy-silty soils		Dokumentnr./Document no. 20190154-09-R
Dokumenttype/Type of document Rapport / Report	Oppdragsgiver/Client Research Council of Norway (RCN)	Dato/Date 2019-12-04
Rettigheter til dokumentet iht kontrakt/ Proprietary rights to the document according to contract NGTS		Rev.nr.&dato/Rev.no.&date 0
Distribusjon/Distribution ÅPEN: Skal tilgjengeliggjøres i åpent arkiv (BRAGE) / OPEN: To be published in open archives (BRAGE)		
Emneord/Keywords Norwegian GeoTest Sites,		

Stedfesting/Geographical information	
Land, fylke/Country Norge, Trøndelag	Havområde/Offshore area
Kommune/Municipality Trondheim	Felt navn/Field name
Sted/Location Øysand	Sted/Location
Kartblad/Map	Felt, blokknr./Field, Block No.
UTM-koordinater/UTM-coordinates Zone: East: North:	Koordinater/Coordinates Projection, datum: East: North:

Dokumentkontroll/Document control					
Kvalitetssikring i henhold til/Quality assurance according to NS-EN ISO9001					
Rev/ Rev.	Revisjonsgrunnlag/Reason for revision	Egenkontroll av/ Self review by:	Sidemanns- kontroll av/ Colleague review by:	Uavhengig kontroll av/ Independent review by:	Tverrfaglig kontroll av/ Interdisciplinary review by:
0	Original document	2019-12-04 Jean-Sebastien L'Heureux	2019-12-04 Priscilla Paniagua		

Dokument godkjent for utsendelse/ Document approved for release	Dato/Date 4 December 2019	Prosjektleder/Project Manager Jean-Sebastien L'Heureux
--	-------------------------------------	--

